

ON THE NUMERICAL EVALUATION OF ALGEBRO-GEOMETRIC SOLUTIONS TO INTEGRABLE EQUATIONS

C. KALLA AND C. KLEIN

ABSTRACT. Physically meaningful periodic solutions to certain integrable partial differential equations are given in terms of multi-dimensional theta functions associated to real Riemann surfaces. Typical analytical problems in the numerical evaluation of these solutions are studied. In the case of hyperelliptic surfaces efficient algorithms exist even for almost degenerate surfaces. This allows the numerical study of solitonic limits. For general real Riemann surfaces, the choice of a homology basis adapted to the anti-holomorphic involution is important for a convenient formulation of the solutions and smoothness conditions. Since existing algorithms for algebraic curves produce a homology basis not related to automorphisms of the curve, we study symplectic transformations to an adapted basis and give explicit formulae for M-curves. As examples we discuss solutions of the Davey-Stewartson and the multi-component nonlinear Schrödinger equations.

1. INTRODUCTION

The importance of Riemann surfaces for the construction of almost periodic solutions to various integrable partial differential equations (PDEs) was realized at the beginning of the 1970s by Novikov, Dubrovin and Its, Matveev. The latter found the Its-Matveev formula for the Korteweg-de Vries (KdV) equation in terms of multi-dimensional theta functions on hyperelliptic Riemann surfaces. Similar formulae were later obtained for other integrable PDEs as nonlinear Schrödinger (NLS) and sine-Gordon equations. For the history of the topic the reader is referred to the reviews [2] and [9]. Krichever [21] showed that theta-functional solutions to the Kadomtsev-Petviashvili equation can be obtained on arbitrary Riemann surfaces. The problems of real-valuedness and smoothness of these solutions were solved by Dubrovin and Natanzon in [11].

Novikov criticized the practical relevance of theta functions since no numerical algorithms existed at the time to actually compute the found solutions. He suggested an effective treatment of theta functions (see, for instance, [9]) by a suitable parametrization of the characteristic quantities of a Riemann surface, i.e., the periods of holomorphic and certain meromorphic differentials on the given surface. This program is limited to genera smaller than 4 since so-called Schottky relations exist for higher genus between the components of the period matrix of a Riemann surface. The task to find such relations is known as the Schottky problem. This led to the famous Novikov conjecture for the Schottky problem that a Riemann matrix (a symmetric matrix with negative definite real part) is the matrix of \mathcal{B} -periods of the normalized holomorphic differentials of a Riemann surface

Date: October 27, 2018.

We thank D. Korotkin and V. Shramchenko for useful discussions and hints. This work has been supported in part by the project FroM-PDE funded by the European Research Council through the Advanced Investigator Grant Scheme, the Conseil Régional de Bourgogne via a FABER grant and the ANR via the program ANR-09-BLAN-0117-01.

if and only if Krichever's formula with this matrix yields a solution to the KP equation. The conjecture was finally proven by Shiota [26].

First plots of KP solutions appeared in [24] and via Schottky uniformizations in [4]. Since all compact Riemann surfaces can be defined via non-singular plane algebraic curves of the form

$$(1.1) \quad F(x, y) := \sum_{n=1}^N \sum_{m=1}^M a_{nm} x^m y^n = 0, \quad x, y \in \mathbb{C},$$

with constant complex coefficients a_{nm} , Deconinck and van Hoeij developed an approach to the symbolic-numerical treatment of algebraic curves. This approach is distributed as the *algcurves* package with Maple, see [6, 7, 8]. A purely numerical approach to real hyperelliptic Riemann surfaces was given in [14, 15], and for general Riemann surfaces in [16]. For a review on computational approaches to Riemann surfaces the reader is referred to [3].

In this paper we want to address typical analytical problems appearing in the numerical study of theta-functional solutions to integrable PDEs, and present the state of the art of the field by considering concrete examples. The case of hyperelliptic Riemann surfaces ($N = 2$ in (1.1)) is the most accessible, since equation (1.1) can be solved explicitly for y , and since a basis for differentials and homology can be given a priori. Families of hyperelliptic curves can be conveniently parametrized by their branch points. The codes [14, 15] are able to treat effectively numerically collisions of branch points, a limit in which certain periods of the corresponding hyperelliptic surface diverge. If the limiting Riemann surface has genus 0, the theta series breaks down to a finite sum which gives for an appropriate choice of the characteristic well known solitonic solutions to the studied equation.

For solutions defined on general real algebraic curves, i.e., curves (1.1) with all a_{nm} real, an important point in applications are reality and smoothness conditions. These are conveniently formulated for a homology basis for which the \mathcal{A} -cycles are invariant under the action of the anti-holomorphic involution. However, the existing algorithms for the computational treatment of algebraic curves produce a basis of the homology that is in general not related to possible automorphisms of the curve. To implement the reality and smoothness requirements, a transformation to the basis for which the conditions are formulated has to be constructed. We study the necessary symplectic transformations and give explicit relations for so-called M-curves, curves with the maximal number of real ovals.

To illustrate these concepts, we study for the first time numerically theta-functional solutions to integrable equations from the family of NLS equations, namely, the multi-component nonlinear Schrödinger equation

$$(1.2) \quad i \frac{\partial \psi_j}{\partial t} + \frac{\partial^2 \psi_j}{\partial x^2} + 2 \left(\sum_{k=1}^n s_k |\psi_k|^2 \right) \psi_j = 0, \quad j = 1, \dots, n,$$

denoted by n -NLS^s, where $s = (s_1, \dots, s_n)$, $s_k = \pm 1$, and the $(2 + 1)$ -dimensional Davey-Stewartson (DS) equations,

$$(1.3) \quad \begin{aligned} i \psi_t + \psi_{xx} - \alpha^2 \psi_{yy} + 2(\Phi + \rho |\psi|^2) \psi &= 0, \\ \Phi_{xx} + \alpha^2 \Phi_{yy} + 2\rho |\psi|_{xx}^2 &= 0, \end{aligned}$$

where $\alpha = i$ or $\alpha = 1$ and where $\rho = \pm 1$. Both equations (1.2) and (1.3) reduce to the NLS equation under certain conditions: the former obviously in the case $n = 1$, the latter

if ψ is independent of the variable y and satisfies certain boundary conditions, for instance that $\Phi + \rho|\psi|^2$ tends to zero when x tends to infinity.

Integrability of the NLS equation was shown by Zakharov and Shabat [31] and algebro-geometric solutions were given by Its [18]. The multi-component nonlinear Schrödinger equation (1.2) in the case $n = 2$, $s = (1, 1)$, is called the vector NLS or Manakov system. Manakov [23] first examined this equation as an asymptotic model for the propagation of the electric field in a waveguide. Its integrability was shown for $n = 2$ by Zakharov and Schulman in [32] and for the general case in [25]. Algebro-geometric solutions to the 2-NLS^s equation with $s = (1, 1)$ were presented in [12], and for the general case in [19]. The DS equation (1.3) was introduced in [5] to describe the evolution of a three-dimensional wave packet on water of finite depth. Its integrability was shown in [1], and solutions in terms of multi-dimensional theta functions on general Riemann surfaces were given in [22, 19].

To ensure the correct numerical implementation of the formulae of [19], we check for each point in the spacetime whether certain identities for theta functions are satisfied. Since these identities are not used in the code, they provide a strong test for the computed quantities. Numerically the identities are never exactly satisfied, but to high precision. The code reports a warning if the residual of the test relations is larger than 10^{-6} which is well below plotting accuracy. Typically the conditions are satisfied to machine precision¹. In addition we compute the solutions on a numerical grid and numerically differentiate them. We check in this way for low genus that the solutions to n -NLS^s and DS in terms of multi-dimensional theta functions satisfy the respective equations to better than 10^{-6} . These two completely independent tests ensure that the presented plots are showing the correct solutions to better than plotting accuracy.

The paper is organized as follows: in Section 2 we recall some facts from the theory of multi-dimensional theta functions and the theory of real Riemann surfaces, necessary to give theta-functional solutions to the n -NLS^s and DS equations. In Section 3 we consider the hyperelliptic case and study concrete examples of low genus, also in almost degenerate situations. In Section 4 we consider examples of non-hyperelliptic real Riemann surfaces and discuss symplectic transformations needed to obtain smooth solutions. We add some concluding remarks in Section 5.

2. THETA FUNCTIONS AND REAL RIEMANN SURFACES

In this section we recall basic facts on Riemann surfaces, in particular real surfaces, and multi-dimensional theta functions defined on them. Solutions to the n -NLS^s and the DS equations in terms of theta functions will be given following [19].

2.1. Theta functions. Let \mathcal{R}_g be a compact Riemann surface of genus $g > 0$. Denote by $(\mathcal{A}, \mathcal{B}) := (\mathcal{A}_1, \dots, \mathcal{A}_g, \mathcal{B}_1, \dots, \mathcal{B}_g)$ a canonical homology basis, and by $(\omega_1, \dots, \omega_g)$ the basis of holomorphic differentials normalized via

$$(2.1) \quad \int_{\mathcal{A}_k} \omega_j = 2i\pi\delta_{kj}, \quad k, j = 1, \dots, g.$$

The matrix \mathbb{B} with entries $\mathbb{B}_{kj} = \int_{\mathcal{B}_k} \omega_j$ of \mathcal{B} -periods of the normalized holomorphic differentials ω_j , $j = 1, \dots, g$, is symmetric and has a negative definite real part. The theta

¹We work with double precision, i.e., a precision of 10^{-16} ; due to rounding errors this is typically reduced to 10^{-12} to 10^{-14} .

function with (half integer) characteristic $\delta = [\delta_1, \delta_2]$ is defined by

$$(2.2) \quad \Theta_{\mathbb{B}}[\delta](\mathbf{z}) = \sum_{\mathbf{m} \in \mathbb{Z}^g} \exp \left\{ \frac{1}{2} \langle \mathbb{B}(\mathbf{m} + \delta_1), \mathbf{m} + \delta_1 \rangle + \langle \mathbf{m} + \delta_1, \mathbf{z} + 2i\pi\delta_2 \rangle \right\},$$

for any $\mathbf{z} \in \mathbb{C}^g$; here $\delta_1, \delta_2 \in \{0, \frac{1}{2}\}^g$ are the vectors of the characteristic δ ; $\langle \cdot, \cdot \rangle$ denotes the scalar product $\langle \mathbf{u}, \mathbf{v} \rangle = \sum_i u_i v_i$ for any $\mathbf{u}, \mathbf{v} \in \mathbb{C}^g$. The theta function $\Theta[\delta](\mathbf{z})$ is even if the characteristic δ is even, i.e., if $4 \langle \delta_1, \delta_2 \rangle$ is even, and odd if the characteristic δ is odd, i.e., if $4 \langle \delta_1, \delta_2 \rangle$ is odd. An even characteristic is called non-singular if $\Theta[\delta](0) \neq 0$, and an odd characteristic is called non-singular if the gradient $\nabla \Theta[\delta](0)$ is non-zero. The theta function with characteristic is related to the theta function with zero characteristic (the Riemann theta function denoted by Θ) as follows

$$(2.3) \quad \Theta[\delta](\mathbf{z}) = \Theta(\mathbf{z} + 2i\pi\delta_2 + \mathbb{B}\delta_1) \exp \left\{ \frac{1}{2} \langle \mathbb{B}\delta_1, \delta_1 \rangle + \langle \mathbf{z} + 2i\pi\delta_2, \delta_1 \rangle \right\}.$$

Denote by Λ the lattice $\Lambda = \{2i\pi\mathbf{N} + \mathbb{B}\mathbf{M}, \mathbf{N}, \mathbf{M} \in \mathbb{Z}^g\}$ generated by the \mathcal{A} and \mathcal{B} -periods of the normalized holomorphic differentials $\omega_j, j = 1, \dots, g$. The complex torus $J(\mathcal{R}_g) = \mathbb{C}^g / \Lambda$ is called the Jacobian of the Riemann surface \mathcal{R}_g . The theta function (2.2) has the following quasi-periodicity property with respect to the lattice Λ :

$$(2.4) \quad \begin{aligned} & \Theta[\delta](\mathbf{z} + 2i\pi\mathbf{N} + \mathbb{B}\mathbf{M}) \\ &= \Theta[\delta](\mathbf{z}) \exp \left\{ -\frac{1}{2} \langle \mathbb{B}\mathbf{M}, \mathbf{M} \rangle - \langle \mathbf{z}, \mathbf{M} \rangle + 2i\pi(\langle \delta_1, \mathbf{N} \rangle - \langle \delta_2, \mathbf{M} \rangle) \right\}. \end{aligned}$$

For the formulation of solutions to physically relevant integrable equations in terms of multi-dimensional theta functions, there is typically a preferred homology basis in which the solution takes a simple form. Let $(\mathcal{A}, \mathcal{B})$ and $(\tilde{\mathcal{A}}, \tilde{\mathcal{B}})$ be arbitrary canonical homology basis defined on \mathcal{R}_g , represented here by $2g$ -dimensional vectors. Under the change of homology basis

$$(2.5) \quad \begin{pmatrix} A & B \\ C & D \end{pmatrix} \begin{pmatrix} \tilde{\mathcal{A}} \\ \tilde{\mathcal{B}} \end{pmatrix} = \begin{pmatrix} \mathcal{A} \\ \mathcal{B} \end{pmatrix},$$

where $\begin{pmatrix} A & B \\ C & D \end{pmatrix} \in Sp(2g, \mathbb{Z})$ is a symplectic matrix, the theta function (2.2) transforms as

$$(2.6) \quad \Theta_{\mathbb{B}}[\delta](\mathbf{z}) = \kappa \sqrt{\det \tilde{\mathbb{K}}} \exp \left\{ \frac{1}{2} \tilde{\mathbf{z}}^t (\tilde{\mathbb{K}}^t)^{-1} B \tilde{\mathbf{z}} \right\} \Theta_{\tilde{\mathbb{B}}}[\tilde{\delta}](\tilde{\mathbf{z}}),$$

where $\tilde{\mathbb{K}} = 2i\pi A + B \tilde{\mathbb{B}}$ and

$$(2.7) \quad \mathbb{B} = 2i\pi(2i\pi C + D \tilde{\mathbb{B}}) \tilde{\mathbb{K}}^{-1},$$

$$(2.8) \quad \tilde{\mathbf{z}} = (2i\pi)^{-1} \tilde{\mathbb{K}}^t \mathbf{z},$$

$$(2.9) \quad \begin{pmatrix} \delta_1 \\ \delta_2 \end{pmatrix} = \begin{pmatrix} A & -B \\ -C & D \end{pmatrix} \begin{pmatrix} \tilde{\delta}_1 \\ \tilde{\delta}_2 \end{pmatrix} + \frac{1}{2} \text{Diag} \begin{pmatrix} B A^t \\ D C^t \end{pmatrix},$$

for any $\mathbf{z} \in \mathbb{C}^g$, where $\text{Diag}(\cdot)$ denotes the column vector of the diagonal entries of the matrix. Here κ is a constant independent of \mathbf{z} and $\tilde{\mathbb{B}}$ (the exact value of κ is not needed for our purposes).

The Abel map $\mathcal{R}_g \rightarrow J(\mathcal{R}_g)$ is defined by

$$(2.10) \quad \int_{p_0}^p := \int_{p_0}^p \omega,$$

for any $p \in \mathcal{R}_g$, where $p_0 \in \mathcal{R}_g$ is the base point of the application, and where $\omega = (\omega_1, \dots, \omega_g)^t$ is the vector of the normalized holomorphic differentials.

Now let k_a denote a local parameter near $a \in \mathcal{R}_g$ and consider the following expansion of the normalized holomorphic differentials ω_j , $j = 1, \dots, g$,

$$(2.11) \quad \omega_j(p) = (V_{a,j} + W_{a,j} k_a(p) + \dots) dk_a(p),$$

for any point $p \in \mathcal{R}_g$ lying in a neighbourhood of a , where $V_{a,j}, W_{a,j} \in \mathbb{C}$. Let us denote by D_a (resp. D'_a) the operator of the directional derivative along the vector $\mathbf{V}_a = (V_{a,1}, \dots, V_{a,g})^t$ (resp. \mathbf{W}_a). According to [24] and [19], the theta function satisfies the following identities derived from Fay's identity [13]:

$$(2.12) \quad D_a D_b \ln \Theta(\mathbf{z}) = q_1 + q_2 \frac{\Theta(\mathbf{z} + \int_a^b) \Theta(\mathbf{z} - \int_a^b)}{\Theta(\mathbf{z})^2},$$

$$(2.13) \quad D'_a \ln \frac{\Theta(\mathbf{z} + \int_a^b)}{\Theta(\mathbf{z})} + D_a^2 \ln \frac{\Theta(\mathbf{z} + \int_a^b)}{\Theta(\mathbf{z})} + \left(D_a \ln \frac{\Theta(\mathbf{z} + \int_a^b)}{\Theta(\mathbf{z})} - K_1 \right)^2 + 2D_a^2 \ln \Theta(\mathbf{z}) + K_2 = 0,$$

for any $\mathbf{z} \in \mathbb{C}^g$ and any distinct points $a, b \in \mathcal{R}_g$; here the scalars q_i, K_i , $i = 1, 2$ depend on the points a, b and are given by

$$(2.14) \quad q_1(a, b) = D_a D_b \ln \Theta[\delta](\int_a^b),$$

$$(2.15) \quad q_2(a, b) = \frac{D_a \Theta[\delta](0) D_b \Theta[\delta](0)}{\Theta[\delta](\int_a^b)^2},$$

$$(2.16) \quad K_1(a, b) = \frac{1}{2} \frac{D'_a \Theta[\delta](0)}{D_a \Theta[\delta](0)} + D_a \ln \Theta[\delta](\int_a^b),$$

$$(2.17) \quad K_2(a, b) = -D'_a \ln \Theta(\int_a^b) - D_a^2 \ln \left(\Theta(\int_a^b) \Theta(0) \right) - \left(D_a \ln \Theta(\int_a^b) - K_1(a, b) \right)^2,$$

where δ is a non-singular odd characteristic.

2.2. Real Riemann surfaces. A Riemann surface \mathcal{R}_g is called real if it admits an anti-holomorphic involution $\tau : \mathcal{R}_g \rightarrow \mathcal{R}_g$, $\tau^2 = \text{id}$. The connected components of the set of fixed points of the anti-involution τ are called real ovals of τ . We denote by $\mathcal{R}_g(\mathbb{R})$ the set of fixed points. According to Harnack's inequality [17], the number k of real ovals of a real Riemann surface of genus g cannot exceed $g + 1$: $0 \leq k \leq g + 1$. Curves with the maximal number $k = g + 1$ of real ovals are called M-curves.

The complement $\mathcal{R}_g \setminus \mathcal{R}_g(\mathbb{R})$ has either one or two connected components. The curve \mathcal{R}_g is called a *dividing* curve if $\mathcal{R}_g \setminus \mathcal{R}_g(\mathbb{R})$ has two components, and \mathcal{R}_g is called *non-dividing* if $\mathcal{R}_g \setminus \mathcal{R}_g(\mathbb{R})$ is connected (notice that an M-curve is always a dividing curve).

Example 2.1. Consider the hyperelliptic curve of genus g defined by the equation

$$(2.18) \quad \mu^2 = \prod_{i=1}^{2g+2} (\lambda - \lambda_i),$$

where the branch points $\lambda_i \in \mathbb{R}$ are ordered such that $\lambda_1 < \dots < \lambda_{2g+2}$. On such a curve, we can define two anti-holomorphic involutions τ_1 and τ_2 , given respectively by $\tau_1(\lambda, \mu) = (\bar{\lambda}, \bar{\mu})$ and $\tau_2(\lambda, \mu) = (\bar{\lambda}, -\bar{\mu})$. Projections of real ovals of τ_1 on the λ -plane coincide with the intervals $[\lambda_{2g+2}, \lambda_1], \dots, [\lambda_{2g}, \lambda_{2g+1}]$, whereas projections of real ovals of τ_2 on the λ -plane coincide with the intervals $[\lambda_1, \lambda_2], \dots, [\lambda_{2g+1}, \lambda_{2g+2}]$. Hence the curve (2.18) is an M-curve with respect to both anti-involutions τ_1 and τ_2 .

Let $(\mathcal{A}, \mathcal{B})$ be a basis of the homology group $H_1(\mathcal{R}_g)$. According to Proposition 2.2 in Vinnikov's paper [30], there exists a canonical homology basis (that we call for simplicity 'Vinnikov basis' in the following) such that

$$(2.19) \quad \begin{pmatrix} \tau\mathcal{A} \\ \tau\mathcal{B} \end{pmatrix} = \begin{pmatrix} \mathbb{I}_g & 0 \\ \mathbb{H} & -\mathbb{I}_g \end{pmatrix} \begin{pmatrix} \mathcal{A} \\ \mathcal{B} \end{pmatrix},$$

where \mathbb{I}_g is the $g \times g$ unit matrix, and \mathbb{H} is a block diagonal $g \times g$ matrix, defined as follows:

1) if $\mathcal{R}_g(\mathbb{R}) \neq \emptyset$,

$$\mathbb{H} = \begin{pmatrix} 0 & 1 & & & & & & & & \\ 1 & 0 & & & & & & & & \\ & & \ddots & & & & & & & \\ & & & 0 & 1 & & & & & \\ & & & 1 & 0 & & & & & \\ & & & & & 0 & & & & \\ & & & & & & \ddots & & & \\ & & & & & & & & \ddots & \\ & & & & & & & & & 0 \end{pmatrix} \quad \text{if } \mathcal{R}_g \text{ is dividing,}$$

$$\mathbb{H} = \begin{pmatrix} 1 & & & & & & & & & \\ & \ddots & & & & & & & & \\ & & 1 & & & & & & & \\ & & & 0 & & & & & & \\ & & & & & \ddots & & & & \\ & & & & & & & & \ddots & \\ & & & & & & & & & 0 \end{pmatrix} \quad \text{if } \mathcal{R}_g \text{ is non-dividing;}$$

$\text{rank}(\mathbb{H}) = g + 1 - k$ in both cases.

2) if $\mathcal{R}_g(\mathbb{R}) = \emptyset$, (i.e. the curve does not have real oval), then

$$\mathbb{H} = \begin{pmatrix} 0 & 1 & & & & & & & & \\ 1 & 0 & & & & & & & & \\ & & \ddots & & & & & & & \\ & & & 0 & 1 & & & & & \\ & & & 1 & 0 & & & & & \end{pmatrix} \quad \text{or} \quad \mathbb{H} = \begin{pmatrix} 0 & 1 & & & & & & & & \\ 1 & 0 & & & & & & & & \\ & & \ddots & & & & & & & \\ & & & & & & 0 & 1 & & \\ & & & & & & 1 & 0 & & \\ & & & & & & & & & 0 \end{pmatrix};$$

$\text{rank}(\mathbb{H}) = g$ if g is even, $\text{rank}(\mathbb{H}) = g - 1$ if g is odd.

Now let us choose the canonical homology basis in $H_1(\mathcal{R}_g)$ satisfying (2.19), take $a, b \in \mathcal{R}_g$ and assume that $\tau a = a$ and $\tau b = b$. Denote by ℓ a contour connecting the points a and b which does not intersect the canonical homology basis. Then the action of τ on the generators $(\mathcal{A}, \mathcal{B}, \ell)$ of the relative homology group $H_1(\mathcal{R}_g, \{a, b\})$ is given by

$$(2.20) \quad \begin{pmatrix} \tau\mathcal{A} \\ \tau\mathcal{B} \\ \tau\ell \end{pmatrix} = \begin{pmatrix} \mathbb{I}_g & 0 & 0 \\ \mathbb{H} & -\mathbb{I}_g & 0 \\ \mathbf{N}^t & \mathbf{M}^t & 1 \end{pmatrix} \begin{pmatrix} \mathcal{A} \\ \mathcal{B} \\ \ell \end{pmatrix},$$

where the vectors $\mathbf{N}, \mathbf{M} \in \mathbb{Z}^g$ are related by (see [19])

$$(2.21) \quad 2\mathbf{N} + \mathbb{H}\mathbf{M} = 0.$$

2.3. Theta-functional solutions of the n -NLS^s equation. Algebro-geometric data associated to smooth theta-functional solutions of the n -NLS^s equation (1.2) consist of $\{\mathcal{R}_g, \tau, f, z_a\}$, where \mathcal{R}_g is a compact Riemann surface of genus $g > 0$ dividing with respect to an anti-holomorphic involution τ , and admitting a real meromorphic function f of degree $n + 1$; here $z_a \in \mathbb{R}$ is a non critical value of f such that the fiber $f^{-1}(z_a) = \{a_1, \dots, a_{n+1}\}$ over z_a belongs to the set $\mathcal{R}_g(\mathbb{R})$. Let us choose natural local parameters k_{a_j} near a_j given by the projection map f , namely, $k_{a_j}(p) = f(p) - z_a$ for any point $p \in \mathcal{R}_g$ lying in a neighbourhood of a_j .

Denote by $(\mathcal{A}, \mathcal{B}, \ell_j)$ the generators of the relative homology group $H_1(\mathcal{R}_g, \{a_{n+1}, a_j\})$. Let $\mathbf{d} \in \mathbb{R}^g$ and $\theta \in \mathbb{R}$. Then the following functions ψ_j , $j = 1, \dots, n$, give smooth solutions of the n -NLS^s equation (1.2), see [19],

$$(2.22) \quad \psi_j(x, t) = |A_j| e^{i\theta} \frac{\Theta(\mathbf{Z} - \mathbf{d} + \mathbf{r}_j)}{\Theta(\mathbf{Z} - \mathbf{d})} \exp\{-i(E_j x - F_j t)\},$$

where $|A_j| = |q_2(a_{n+1}, a_j)|^{1/2} \exp\{\frac{1}{2} \langle \mathbf{d}, \mathbf{M}_j \rangle\}$. The vector $\mathbf{M}_j \in \mathbb{Z}^g$ is defined by the action of τ on the relative homology group $H_1(\mathcal{R}_g, \{a_{n+1}, a_j\})$ (see (2.20)). Moreover, $\mathbf{r}_j = \int_{\ell_j} \omega$, and the vector \mathbf{Z} reads

$$\mathbf{Z} = i \mathbf{V}_{a_{n+1}} x + i \mathbf{W}_{a_{n+1}} t,$$

where vectors $\mathbf{V}_{a_{n+1}}$ and $\mathbf{W}_{a_{n+1}}$ are defined in (2.11). The scalars E_j, F_j are given by

$$(2.23) \quad E_j = K_1(a_{n+1}, a_j), \quad F_j = K_2(a_{n+1}, a_j) - 2 \sum_{k=1}^n q_1(a_{n+1}, a_k),$$

and scalars q_i, K_i , $i = 1, 2$ are defined in (2.14)-(2.17). According to [19], necessary conditions for the functions ψ_j in (2.22) to solve the n -NLS^s equation are the identities (2.12) and (2.13) with $(a, b) := (a_{n+1}, a_j)$.

The signs s_1, \dots, s_n in (1.2) are given by

$$(2.24) \quad s_j = \exp\{i\pi(1 + \alpha_j)\},$$

where $\alpha_j \in \mathbb{Z}$ denote certain intersection indices on \mathcal{R}_g defined as follows: let $\tilde{a}_{n+1}, \tilde{a}_j \in \mathcal{R}_g(\mathbb{R})$ lie in a neighbourhood of a_{n+1} and a_j respectively such that $f(\tilde{a}_{n+1}) = f(\tilde{a}_j)$. Denote by $\tilde{\ell}_j$ an oriented contour connecting \tilde{a}_{n+1} and \tilde{a}_j . Then

$$(2.25) \quad \alpha_j = (\tau \tilde{\ell}_j - \tilde{\ell}_j) \circ \ell_j$$

is the intersection index of the closed contour $\tau \tilde{\ell}_j - \tilde{\ell}_j$ and the contour ℓ_j ; this index is computed in the relative homology group $H_1(\mathcal{R}_g, \{a_{n+1}, a_j\})$.

In particular, it was shown in [19] that solutions of the focusing n -NLS^s equation, i.e., for $s = (1, \dots, 1)$, are obtained when the branch points of the meromorphic function f are pairwise conjugate.

2.4. Theta-functional solutions of the DS equations. Now let us introduce smooth solutions of the DS equations. In characteristic coordinates

$$\xi = \frac{1}{2}(x - i\alpha y), \quad \eta = \frac{1}{2}(x + i\alpha y), \quad \alpha = i \text{ or } 1,$$

the DS equations (1.3) take the form

$$(2.26) \quad \begin{aligned} i\psi_t + \frac{1}{2}(\partial_{\xi\xi} + \partial_{\eta\eta})\psi + 2\phi\psi &= 0, \\ \partial_{\xi}\partial_{\eta}\phi + \rho\frac{1}{2}(\partial_{\xi\xi} + \partial_{\eta\eta})|\psi|^2 &= 0, \end{aligned}$$

where $\phi := \Phi + \rho|\psi|^2$, $\rho = \pm 1$. Recall that DS1 $^{\rho}$ denotes the Davey-Stewartson equation when $\alpha = i$ (in this case ξ and η are both real), and DS2 $^{\rho}$ when $\alpha = 1$ (in this case ξ and η are pairwise conjugate).

In both cases, for the DS1 $^{\rho}$ and DS2 $^{\rho}$ equations, the solutions have the form [22, 19]:

$$(2.27) \quad \psi(\xi, \eta, t) = |A| e^{i\theta} \frac{\Theta(\mathbf{Z} - \mathbf{d} + \mathbf{r})}{\Theta(\mathbf{Z} - \mathbf{d})} \exp \left\{ -i \left(G_1 \xi + G_2 \eta - G_3 \frac{t}{2} \right) \right\},$$

$$(2.28) \quad \phi(\xi, \eta, t) = \frac{1}{2} (\ln \Theta(\mathbf{Z} - \mathbf{d}))_{\xi\xi} + \frac{1}{2} (\ln \Theta(\mathbf{Z} - \mathbf{d}))_{\eta\eta} + \frac{h}{4}.$$

Here $\mathbf{r} = \int_a^b \omega$ for some distinct points $a, b \in \mathcal{R}_g$, and the vector \mathbf{Z} is defined as

$$(2.29) \quad \mathbf{Z} = i \left(\kappa_1 \mathbf{V}_a \xi - \kappa_2 \mathbf{V}_b \eta + (\kappa_1^2 \mathbf{W}_a - \kappa_2^2 \mathbf{W}_b) \frac{t}{2} \right).$$

Moreover, the scalars G_1 , G_2 and G_3 read

$$(2.30) \quad G_1 = \kappa_1 K_1(a, b), \quad G_2 = \kappa_2 K_1(b, a),$$

$$(2.31) \quad G_3 = \kappa_1^2 K_2(a, b) + \kappa_2^2 K_2(b, a) + h,$$

where the scalars K_1, K_2 are defined in (2.16) and (2.17). As shown in [19], necessary conditions for the functions ψ (2.27) and ϕ (2.28) to solve the DS equations are the identities (2.12) and (2.13).

Algebro-geometric data associated to smooth solutions (2.27), (2.28) of the DS1 $^{\rho}$ equation consist of $\{\mathcal{R}_g, \tau, a, b, k_a, k_b\}$, where \mathcal{R}_g is a compact Riemann surface of genus $g > 0$, dividing with respect to an anti-holomorphic involution τ , a, b are two distinct points in $\mathcal{R}_g(\mathbb{R})$, and k_a, k_b denote local parameters near a and b respectively which satisfy $\overline{k_a(\tau p)} = k_a(p)$ for any p lying in a neighbourhood of a , and $\overline{k_b(\tau p)} = k_b(p)$ for any p lying in a neighbourhood of b . The remaining quantities satisfy the conditions: $\mathbf{d} \in \mathbb{R}^g$, $\theta, h \in \mathbb{R}$, $\kappa_2 \in \mathbb{R} \setminus \{0\}$, and

$$(2.32) \quad \kappa_1 = -\rho \tilde{\kappa}_1^2 \kappa_2 q_2(a, b) \exp \left\{ \frac{1}{2} \langle \mathbb{B}\mathbf{M}, \mathbf{M} \rangle + \langle \mathbf{r} + \mathbf{d}, \mathbf{M} \rangle \right\},$$

for some $\tilde{\kappa}_1 \in \mathbb{R}$, where $\mathbf{M} \in \mathbb{Z}^g$ is defined in (2.20). The scalar $|A|$ is given by

$$|A| = |\tilde{\kappa}_1 \kappa_2 q_2(a, b)| \exp \{ \langle \mathbf{d}, \mathbf{M} \rangle \},$$

where the quantity q_2 is defined in (2.15).

Algebro-geometric data associated to smooth solutions (2.27), (2.28) of the DS2 $^{\rho}$ equation consist of $\{\mathcal{R}_g, \tau, a, b, k_a, k_b\}$, where \mathcal{R}_g is a compact Riemann surface of genus $g > 0$ with an anti-holomorphic involution τ , a, b are two distinct points such that $\tau a = b$, and k_a, k_b denote local parameters near a and b respectively which satisfy $\overline{k_b(\tau p)} = k_a(p)$ for any point p lying in a neighbourhood of a . Moreover, $\mathbf{d} \in i\mathbb{R}^g$, $\theta, h \in \mathbb{R}$, $\kappa_1, \kappa_2 \in \mathbb{C} \setminus \{0\}$ satisfy $\overline{\kappa_1} = \kappa_2$, and the scalar $|A|$ is given by

$$|A| = |\kappa_1| |q_2(a, b)|^{1/2}.$$

Smooth solutions of the DS2 $^+$ equation are obtained when the curve \mathcal{R}_g is an M-curve with respect to τ , whereas solutions to DS2 $^-$ are smooth if the associated Riemann surface

does not have real oval with respect to τ , and if there is no pseudo-real function of degree $g - 1$ on it (i.e., function which satisfies $\overline{f(\tau p)} = -f(p)^{-1}$), see [22].

Remark 2.1. *The symmetric structure of the DS equations (2.26) with respect to ξ and η implies that a solution $\psi = \Psi(\xi, \eta, t)$ to $DS1^+$ leads to a solution $\Psi(-\xi, \eta, t)$ of $DS1^-$.*

3. HYPERELLIPTIC CASE

Here we consider concrete examples for the solutions, in terms of multi-dimensional theta functions, to DS and n -NLS^s on hyperelliptic Riemann surfaces. We first review the numerical methods to visualize the solutions and discuss how the accuracy is tested.

3.1. Computation on real hyperelliptic curves. The simplest example of algebraic curves are hyperelliptic curves,

$$(3.1) \quad \mu^2 = \begin{cases} \prod_{i=1}^{2g+2} (\lambda - \lambda_i), & \text{without branching at infinity} \\ \prod_{i=1}^{2g+1} (\lambda - \lambda_i), & \text{with branching at infinity} \end{cases},$$

where g is the genus of the Riemann surface, and where we have for the branch points $\lambda_i \in \mathbb{C}$ the relations $\lambda_i \neq \lambda_j$ for $i \neq j$. If the number of finite branch points is odd, the curve is branched at infinity. Recall that all Riemann surfaces of genus 2 are hyperelliptic, and that the involution σ which interchanges the sheets, $\sigma(\lambda, \mu) = (\lambda, -\mu)$, is an automorphism on any hyperelliptic curve in the form (3.1). A vector of holomorphic differentials for these surfaces is given by $(1, \lambda, \dots, \lambda^{g-1})^t d\lambda/\mu$. For a real hyperelliptic curve, the branch points are either real or pairwise conjugate. As we saw in Example 2.1, if all branch points λ_i are real and ordered such that $\lambda_1 < \dots < \lambda_{2g+2}$, the hyperelliptic curve is an M-curve with respect to both anti-holomorphic involutions τ_1 and τ_2 defined in the example. The other case of interest in the context of smooth solutions to n -NLS^s and DS are real curves without real branch point. For the involution τ_1 , a curve given by $\mu^2 = \prod_{i=1}^{g+1} (\lambda - \lambda_i)(\lambda - \bar{\lambda}_i)$, with $\lambda_i \in \mathbb{C} \setminus \mathbb{R}$, $i = 1, \dots, g+1$, in this case is dividing (two points whose projections onto \mathbb{C} have respectively a positive and a negative imaginary part cannot be connected by a contour which does not cross a real oval), whereas a curve given by $\mu^2 = -\prod_{i=1}^{g+1} (\lambda - \lambda_i)(\lambda - \bar{\lambda}_i)$ has no real oval, and vice versa for the involution τ_2 .

In the following, we will only consider real hyperelliptic curves without branching at infinity and write the defining equation in the form $\mu^2 = (\lambda - \xi)(\lambda - \eta) \prod_{i=1}^g (\lambda - E_i)(\lambda - F_i)$. It is possible to introduce a convenient homology basis on the related surfaces, see Fig. 1 for the case $\eta = \bar{\xi}$.

The simple form of the algebraic relation between μ and λ for hyperelliptic curves makes the generation of very efficient numerical codes possible, see, for instance, [14, 15] for details. These codes allow the treatment of almost degenerate Riemann surfaces, i.e., the case where the branch points almost collide pairwise, where the distance of the branch points is of the order of machine precision: $|E_i - F_i| \sim 10^{-14}$. The homology basis Fig. 1 is adapted to this kind of degeneration.

The Abel map $\int_a^b \omega$ between two points a and b is computed in the following way: the sheet identified at the point $a = (\lambda(a), \mu(a))$ (where we take for μ the root computed by Matlab) is labeled sheet 1, and at the point $(\lambda(a), -\mu(a))$, sheet 2. Then the ramification point whose projection to the λ -sphere has the minimal distance to $\lambda(a)$ is determined. For simplicity we assume always that this is the point ξ in Fig. 1 (for another branch point, this leads to the addition of half-periods, see e.g. [2]). This means we compute $\int_a^b \omega$ as $\int_a^b \omega = \int_\xi^b \omega - \int_\xi^a \omega$. The choice of a branch point as the base point of the Abel map has the

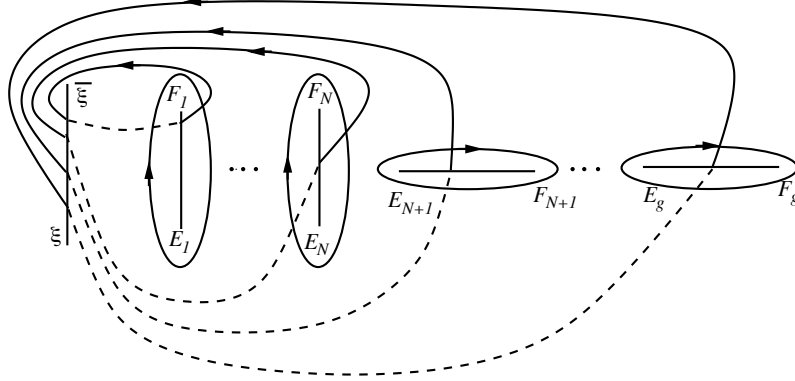


FIGURE 1. Homology basis on real hyperelliptic curves, contours on sheet 1 are solid, contours on sheet 2 are dashed. \mathcal{A} -cycles are the closed contours entirely on sheet 1.

advantage that a change of sheet of a point a just implies a change of sign of the integral: $\int_{\xi}^{(\lambda(a), \mu(a))} \omega = -\int_{\xi}^{(\lambda(a), -\mu(a))} \omega$. To compute the integral $\int_{\xi}^a \omega$, one has to analytically continue μ on the connecting line between $\lambda(a)$ and ξ onto the λ -sphere. Whereas the root μ is not supposed to have any branching on the considered path, the square root in Matlab is branched on the negative real axis. To analytically continue μ on the path $[\lambda(a), \xi]$, we compute the Matlab root at some $\lambda_j \in [\lambda(a), \xi]$, $j = 0, \dots, N_c$ and analytically continue it starting from $\mu(a)$ by demanding that $|\mu(\lambda_{j+1}) - \mu(\lambda_j)| < |\mu(\lambda_{j+1}) + \mu(\lambda_j)|$. The so defined sheets will be denoted here and in the following by numbers, i.e., a point on sheet 1 with projection $\lambda(a)$ into the base is denoted by $(\lambda(a))^{(1)}$.

Thus the computation of the Abel map is reduced to the computation of line integrals on the connecting line between $\lambda(a)$ and ξ in the complex λ -plane. For the numerical computation of such integrals we use Clenshaw-Curtis integration (see, for instance, [27]): to compute an integral $\int_{-1}^1 h(x) dx$, this algorithm samples the integrand on the $N_c + 1$ Chebyshev collocation points $x_j = \cos(j\pi/N_c)$, $j = 0, \dots, N_c$. The integral is approximated as the sum: $\int_{-1}^1 h(x) dx \sim \sum_{j=0}^{N_c} w_j h(x_j)$ (see [27] on how to obtain the weights w_j). It can be shown that the convergence of the integral is exponential for analytic functions h as the ones considered here. To compute the Abel map, one uses the transformation $\lambda \rightarrow \lambda(a)(1+x)/2 + \xi(1-x)/2$, to the Clenshaw-Curtis integration variable. The same procedure is then carried out for the integral from ξ to b .

The theta functions are approximated as in [14] as a sum,

$$(3.2) \quad \Theta_{\mathbb{B}}[\delta](\mathbf{z}) \sim \sum_{m_1=-N_{\theta}}^{N_{\theta}} \dots \sum_{m_g=-N_{\theta}}^{N_{\theta}} \exp \left\{ \frac{1}{2} \langle \mathbb{B}(\mathbf{m} + \delta_1), \mathbf{m} + \delta_1 \rangle + \langle \mathbf{m} + \delta_1, \mathbf{z} + 2i\pi\delta_2 \rangle \right\}.$$

The periodicity properties of the theta function (2.4) make it possible to write $\mathbf{z} = \mathbf{z}_0 + 2i\pi\mathbf{N} + \mathbb{B}\mathbf{M}$ for some $\mathbf{N}, \mathbf{M} \in \mathbb{Z}^g$, where $\mathbf{z}_0 = 2i\pi\alpha + \mathbb{B}\beta$ with $\alpha_i, \beta_i \in]-\frac{1}{2}, \frac{1}{2}]$ for $i = 1, \dots, g$. The value of N_{θ} is determined by the condition that all terms in (2.2) with $|m_i| > N_{\theta}$ are smaller than machine precision, which is controlled by the largest eigenvalue of the real part of the Riemann matrix (the one with minimal absolute value since the real part is negative definite), see [14, 16].

To control the accuracy of the numerical solutions, we use essentially two approaches. First we check the theta identity (2.13), which is the underlying reason for the studied functions being solutions to n -NLS^s and DS, at each point in the spacetime. This test requires the computation of theta derivatives not needed in the solution (which slightly reduces the efficiency of the code since additional quantities are computed), but provides an immediate check whether the solution satisfies (2.13) with the required accuracy. Since this identity is not implemented in the code, it provides a strong test. This ensures that all quantities entering the solution are computed with the necessary precision. In addition, the solutions are computed on Chebyshev collocation points (see, for instance, [27]) for each of the physical variables. This can be used for an expansion of the computed solution in terms of Chebyshev polynomials, a so-called spectral method having in practice exponential convergence for analytic functions as the ones considered here. Since the derivatives of the Chebyshev polynomials can be expressed linearly in terms of Chebyshev polynomials, a derivative acts on the space of polynomials via a so called differentiation matrix. With these standard Chebyshev differentiation matrices (see [27]), the solution can be numerically differentiated. The computed derivatives allow to check with which numerical precision the PDE is satisfied by a numerical solution. With these two independent tests, we ensure that the shown solutions are correct to much better than plotting accuracy (the code reports a warning if the above tests are not satisfied to better than 10^{-6}).

3.2. Solutions to the DS equations. The elliptic solutions are the well known travelling wave solutions and will not be discussed here. The simplest examples we will consider for the DS solutions are given on hyperelliptic curves of genus 2. As we saw in Section 2.4, for DS1 ^{ρ} reality and smoothness conditions imply that the branch points of the curve are either all real (M-curve) or all pairwise conjugate (dividing curve). The points a and b must project to real points on the λ -sphere and must be stable under the anti-holomorphic involution τ (we use here $\tau = \tau_1$, as defined in Example 2.1, except for DS2⁻). For DS2 ^{ρ} , we have $\tau a = b$ where the projection of a onto the λ -sphere is the conjugate of the projection of b . For DS2⁺ the curve must have only real branch points (M-curve), whereas for DS2⁻ it must have no real oval.

For DS we will mainly give plots for fixed time since for low genus, the solution is essentially travelling in one direction. For higher genus, we show a more interesting time dependence in Fig. 9.

We first consider the defocusing variants, DS1⁺ and DS2⁺ on M-curves. In genus 2 we study the family of curves with the branch points $-2, -1, 0, \epsilon, 2, 2 + \epsilon$ for $\epsilon = 1$ and $\epsilon = 10^{-10}$. In the former case the solutions will be periodic in the (x, y) -plane, in the latter almost solitonic since the Riemann surface is almost degenerate (in the limit $\epsilon \rightarrow 0$ the surface degenerates to a surface of genus 0; the resulting solutions are discussed in more detail in [20]). To obtain non-trivial solutions in the solitonic limit, we use $\mathbf{d} = \frac{1}{2} \begin{bmatrix} 1 & 1 \\ 0 & 0 \end{bmatrix}^t$ in all examples. In Fig. 2 it can be seen that these are in fact *dark solitons*, i.e., the solutions tend asymptotically to a non-zero constant and the solitons thus represent ‘shadows’ on a background of light. The well known features from soliton collisions for (1+1)-dimensional integrable equations, namely, the propagation without change of shape, and the unchanged shape and phase shift after the collision, can be seen here in the (x, y) -plane.

The corresponding solutions to DS2⁺ can be seen in Fig. 3. We only show the square modulus of the solution here for simplicity. For the real and the imaginary part of such a solution for the DS1⁻-case, see Fig. 6. Because of remark 2.1 all solutions shown for DS1⁺

on M-curves are after the change of coordinate $\xi \rightarrow -\xi$ solutions to $DS1^-$. For this reason $DS1^-$ solutions on M-curves will not be presented here.

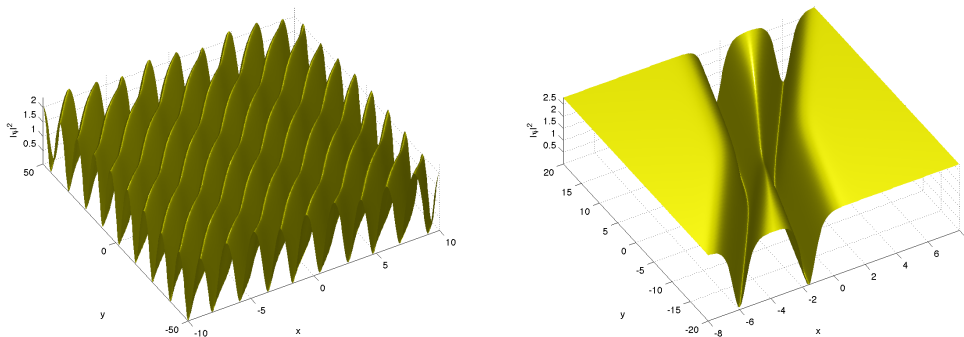


FIGURE 2. Solution (2.27) to the $DS1^+$ equation at $t = 0$ on a hyperelliptic curve of genus 2 with branch points $-2, -1, 0, \epsilon, 2, 2 + \epsilon$ and $a = (-1.9)^{(1)}$, $b = (-1.1)^{(2)}$ for $\epsilon = 1$ on the left and $\epsilon = 10^{-10}$, the almost solitonic limit, on the right.

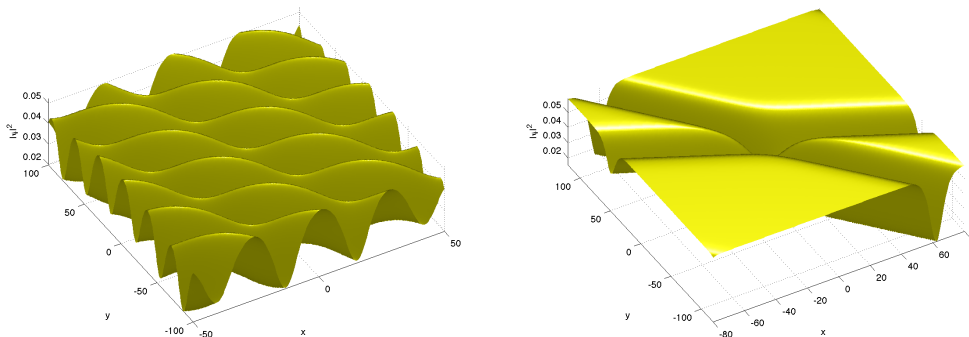


FIGURE 3. Solution (2.27) to the $DS2^+$ equation at $t = 0$ on a hyperelliptic curve of genus 2 with branch points $-2, -1, 0, \epsilon, 2, 2 + \epsilon$ and $a = (-1.5 + 2i)^{(1)}$, $b = (-1.5 - 2i)^{(2)}$ for $\epsilon = 1$ on the left and $\epsilon = 10^{-10}$, the almost solitonic limit, on the right.

In the same way one can study, on a genus 4 hyperelliptic curve, the formation of the dark 4-soliton for these two equations. We consider the curve with branch points $-4, -3, -2, -2 + \epsilon, 0, \epsilon, 2, 2 + \epsilon, 4, 4 + \epsilon$ for $\epsilon = 1$ and $\epsilon = 10^{-10}$, and use $\mathbf{d} = \frac{1}{2} \begin{bmatrix} 1 & 1 & 1 & 1 \\ 0 & 0 & 0 & 0 \end{bmatrix}^t$. The $DS1^+$ solutions for this curve can be seen in Fig. 4. The corresponding solutions to $DS2^+$ is shown in Fig. 5.

Solutions to the focusing variants of these equations can be obtained on hyperelliptic curves with pairwise conjugate branch points. For such solutions the solitonic limit cannot be obtained as above since the quotient of theta functions in (2.27) tends to a constant in this case. To obtain the well-known *bright solitons* (solutions tend to zero at spatial infinity) in this way, the hyperelliptic curve has to be completely degenerated (all branch

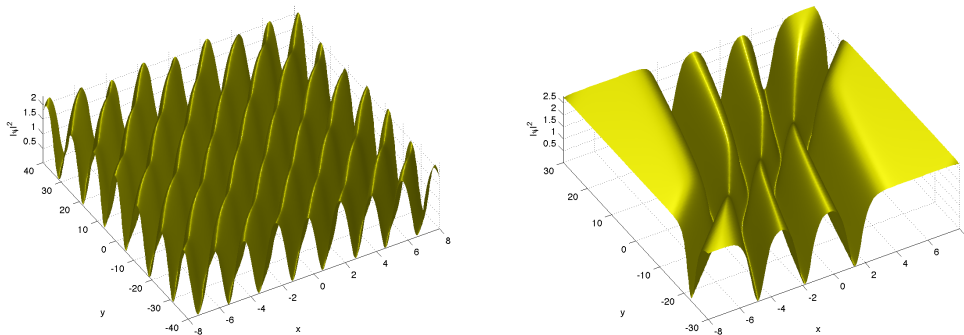


FIGURE 4. Solution (2.27) to the $DS1^+$ equation at $t = 0$ on a hyperelliptic curve of genus 4 with branch points $-4, -3, -2, -2 + \epsilon, 0, \epsilon, 2, 2 + \epsilon, 4, 4 + \epsilon$ and $a = (-3.9)^{(1)}$, $b = (-3.1)^{(2)}$ for $\epsilon = 1$ on the left and $\epsilon = 10^{-10}$, the almost solitonic limit, on the right.

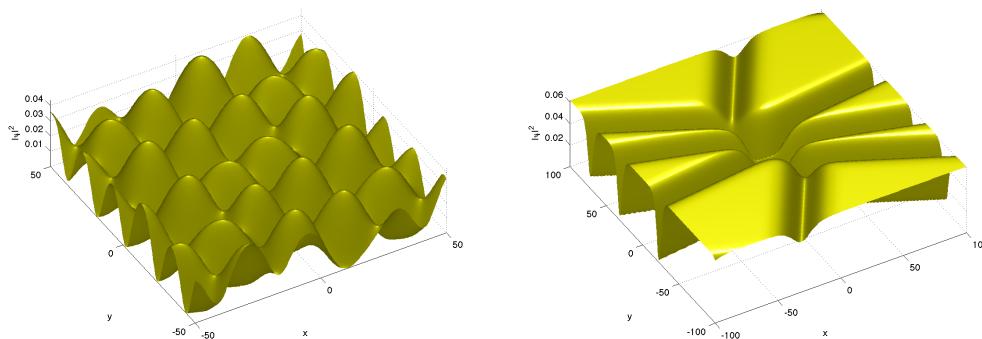


FIGURE 5. Solution (2.27) to the $DS2^+$ equation at $t = 0$ on a hyperelliptic curve of genus 4 with branch points $-4, -3, -2, -2 + \epsilon, 0, \epsilon, 2, 2 + \epsilon, 4, 4 + \epsilon$ and $a = (-1.5 + 2i)^{(1)}$, $b = (-1.5 - 2i)^{(1)}$ for $\epsilon = 1$ on the left and $\epsilon = 10^{-10}$, the almost solitonic limit, on the right.

points must collide pairwise to double points) which leads to limits of the form '0/0' in the expression for the solution (2.27) which are not convenient for a numerical treatment; see [20] for an analytic discussion. Therefore we only consider non-degenerate hyperelliptic curves here. To obtain smooth solutions, we use $\mathbf{d} = 0$. A solution in genus 2 of the $DS1^-$ equation is studied on the curve with the branch points $-2 \pm i, -1 \pm i, 1 \pm i$ in Fig. 6.

A typical example of a $DS1^-$ solution on a hyperelliptic curve of genus 4 with branch points $-2 \pm i, -1 \pm i, \pm i, 1 \pm i, 2 \pm i$ is shown in Fig. 7.

Smooth solutions to $DS2^-$ can be obtained on Riemann surfaces without real oval for points a and b satisfying $\tau a = b$. As mentioned above, hyperelliptic curves of the form $\mu^2 = -\prod_{i=1}^{2g+2}(\lambda - \lambda_i)$ with pairwise conjugate branch points have no real oval for the standard involution τ_1 as defined in Example 2.1. On the other hand, surfaces defined by the algebraic equation $\mu^2 = \prod_{i=1}^{2g+2}(\lambda - \lambda_i)$ have no real oval for the involution τ_2 (see Example 2.1). We will consider here τ_2 for the same curves as for $DS1^-$. An example for

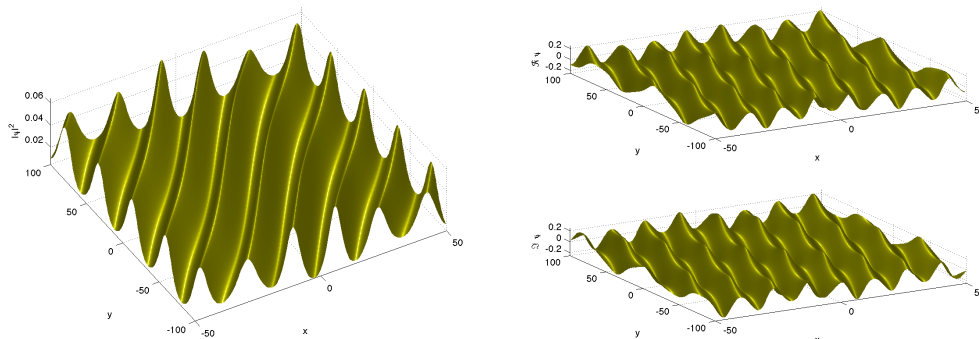


FIGURE 6. Solution (2.27) to the $DS1^-$ equation at $t = 0$ on a hyperelliptic curve of genus 2 with branch points $-2 \pm i$, $-1 \pm i$, $1 \pm i$ and $a = (-4)^{(1)}$, $b = (-3)^{(2)}$. The square modulus of the solution is shown on the left, real and imaginary parts on the right.

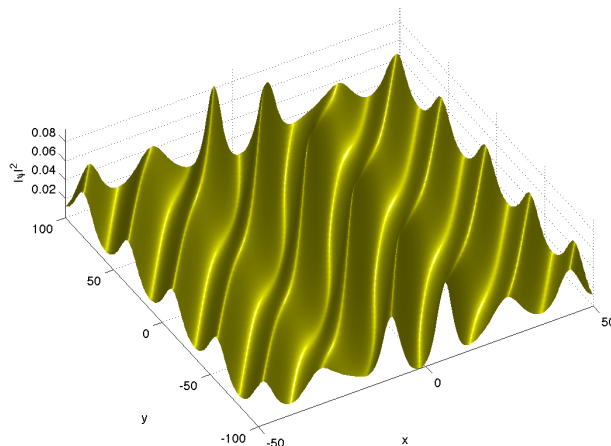


FIGURE 7. Solution (2.27) to the $DS1^-$ equation at $t = 0$ on a hyperelliptic curve of genus 4 with branch points $-2 \pm i$, $-1 \pm i$, $\pm i$, $1 \pm i$, $2 \pm i$ and $a = (-4)^{(1)}$, $b = (-3)^{(2)}$.

genus 2 can be seen in Fig. 8. An example for a $DS2^-$ solution of genus 4 can be seen in Fig. 9.

3.3. Solutions to the n -NLS^s equation. A straightforward way to obtain solutions (2.22) to the n -NLS^s equation is given on an $(n + 1)$ -sheeted branched covering of the complex plane, an approach that will be studied in more detail in the next section. As can be seen from the proof of Theorem 4.1 in [19], the crucial point in the construction of these solutions is the fact that $\sum_{k=1}^{n+1} \mathbf{V} a_k = 0$. This implies that it is also possible to construct theta-functional n -NLS^s solutions on hyperelliptic surfaces by introducing constants γ_k via $\sum_{k=1}^{n+1} \gamma_k \mathbf{V} a_k = 0$ in the following corollary of Theorem 4.1 in [19]:

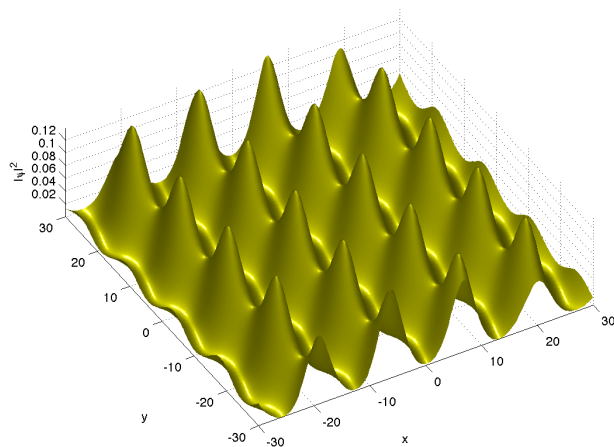


FIGURE 8. Solution to the $DS2^-$ equation at $t = 0$ on a hyperelliptic curve of genus 2 with branch points $-2 \pm i$, $-1 \pm i$, $1 \pm i$ and $a = (-1.5 + 2i)^{(1)}$, $b = (-1.5 - 2i)^{(2)}$.

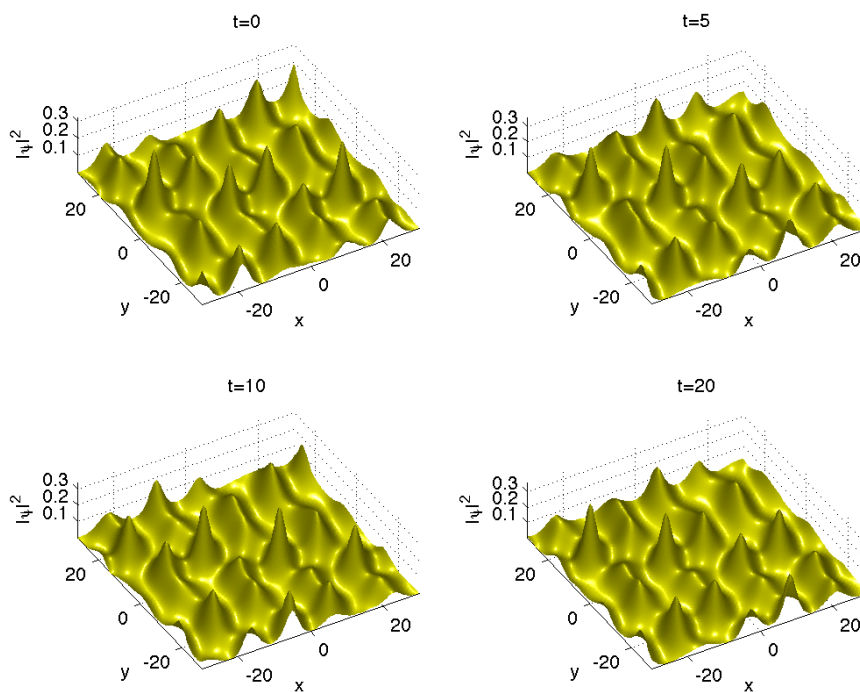


FIGURE 9. Solution to the $DS2^-$ equation for several values of t on a hyperelliptic curve of genus 4 with branch points $-2 \pm i$, $-1 \pm i$, $\pm i$, $1 \pm i$, $2 \pm i$ and $a = (-1.5 + 2i)^{(1)}$, $b = (-1.5 - 2i)^{(2)}$.

Corollary 3.1. *Let \mathcal{R}_g be a real hyperelliptic curve of genus $g > 0$ and denote by τ an anti-holomorphic involution. Choose the canonical homology basis which satisfies (2.19). Take $n \geq g$ and let $a_1, \dots, a_{n+1} \in \mathcal{R}_g(\mathbb{R})$ not ramification points having distinct projection $\lambda(a_j)$, $j = 1, \dots, n+1$, onto the λ -sphere. Denote by ℓ_j an oriented contour between a_{n+1} and a_j which does not intersect cycles of the canonical homology basis. Let $\mathbf{d}_R \in \mathbb{R}^g$, $\mathbf{T} \in \mathbb{Z}^g$, and define $\mathbf{d} = \mathbf{d}_R + \frac{i\pi}{2}(\text{diag}(\mathbb{H}) - 2\mathbf{T})$. Take $\theta \in \mathbb{R}$ and let $\gamma_{g+1}, \dots, \gamma_n \in \mathbb{R}$ be arbitrary constants with $\gamma_{n+1} = 1$. Put $\hat{s} = (\text{sign}(\gamma_1) s_1, \dots, \text{sign}(\gamma_n) s_n)$ where s_j is given in (2.24), and the scalars γ_j , $j = 1, \dots, g$, are defined by $\sum_{k=1}^{n+1} \gamma_k \mathbf{V}_{a_k} = 0$. Then the following functions ψ_j , $j = 1, \dots, n$, give solutions of the n -NLS $^{\hat{s}}$ equation (1.2)*

$$(3.3) \quad \psi_j(x, t) = |\gamma_j|^{1/2} |A_j| e^{i\theta} \frac{\Theta(\mathbf{Z} - \mathbf{d} + \mathbf{r}_j)}{\Theta(\mathbf{Z} - \mathbf{d})} \exp\{-i(E_j x - F_j t)\},$$

where $|A_j| = |q_2(a_{n+1}, a_j)|^{1/2} \exp\{\frac{1}{2} \langle \mathbf{d}, \mathbf{M}_j \rangle\}$. Here $\mathbf{Z} = i \mathbf{V}_{a_{n+1}} x + i \mathbf{W}_{a_{n+1}} t$, where the vectors $\mathbf{V}_{a_{n+1}}$ and $\mathbf{W}_{a_{n+1}}$ were introduced in (2.11), and $\mathbf{r}_j = \int_{\ell_j} \omega$. The scalars E_j, F_j are given by

$$E_j = K_1(a_{n+1}, a_j), \quad F_j = K_2(a_{n+1}, a_j) - 2 \sum_{k=1}^n \gamma_k q_1(a_{n+1}, a_k),$$

where q_i, K_i for $i = 1, 2$ are defined in (2.14)-(2.17). If \mathcal{R}_g is dividing and if $\mathbf{d} \in \mathbb{R}^g$, functions (3.3) give smooth solutions of n -NLS $^{\hat{s}}$.

As an example we consider, as for DS in genus 2, the family of curves with the branch points $-2, -1, 0, \epsilon, 2, 2 + \epsilon$ for $\epsilon = 1$ and $\epsilon = 10^{-10}$. In the former case the solutions will be periodic in the (x, t) -plane, in the latter almost solitonic. To obtain non-trivial solutions in the solitonic limit, we use $\mathbf{d} = \frac{1}{2} \begin{bmatrix} 1 & 1 \\ 0 & 0 \end{bmatrix}^t$ in all examples.

In Fig. 10 we show the case $a_1 = (-1.9)^{(1)}$, $a_2 = (-1.1)^{(1)}$ and $a_3 = (-1.8)^{(1)}$, which leads to a solution of 2-NLS $^{\hat{s}}$ with $\hat{s} = (-1, -1)$. Interchanging a_2 and a_3 in the above example, we obtain a solution to 2-NLS $^{\hat{s}}$ with $\hat{s} = (1, -1)$ in Fig. 11.

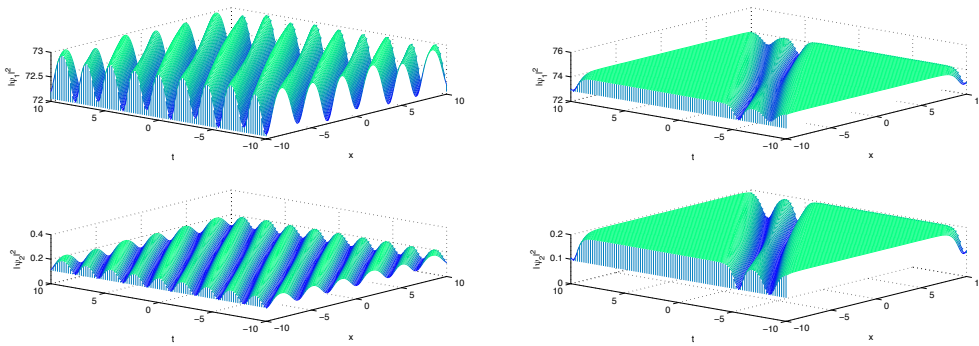


FIGURE 10. *Solution (3.3) to the 2-NLS $^{\hat{s}}$ equation with $\hat{s} = (-1, -1)$ on a hyperelliptic curve of genus 2 with branch points $-2, -1, 0, \epsilon, 2, 2 + \epsilon$ and $a_1 = (-1.9)^{(1)}$, $a_2 = (-1.1)^{(1)}$ and $a_3 = (-1.8)^{(1)}$ for $\epsilon = 1$ on the left and $\epsilon = 10^{-10}$, the almost solitonic limit, on the right.*

Solutions of 4-NLS $^{\hat{s}}$ can be studied in the same way on the hyperelliptic curve of genus 4 with branch points $-4, -3, -2, -2 + \epsilon, 0, \epsilon, 2, 2 + \epsilon, 4, 4 + \epsilon$. We use $\mathbf{d} = \frac{1}{2} \begin{bmatrix} 1 & 1 & 1 & 1 \\ 0 & 0 & 0 & 0 \end{bmatrix}^t$ and the

points $a_1 = (-3.9)^{(1)}$, $a_2 = (-3.7)^{(1)}$, $a_3 = (-3.5)^{(1)}$, $a_4 = (-3.3)^{(1)}$ and $a_5 = (-3.1)^{(1)}$. Since the vectors \mathbf{V}_{a_j} and \mathbf{W}_{a_j} are very similar in this case, the same is true for the functions ψ_j . Therefore, we will only show the square modulus of the first component ψ_1 in Fig. 12 for $\hat{s} = (1, -1, 1, -1)$ on the left. Interchanging a_4 and a_5 in this case, one gets a solution to 4-NLS $^{\hat{s}}$ with $\hat{s} = (-1, 1, -1, -1)$ which can be seen on the right of Fig. 12.

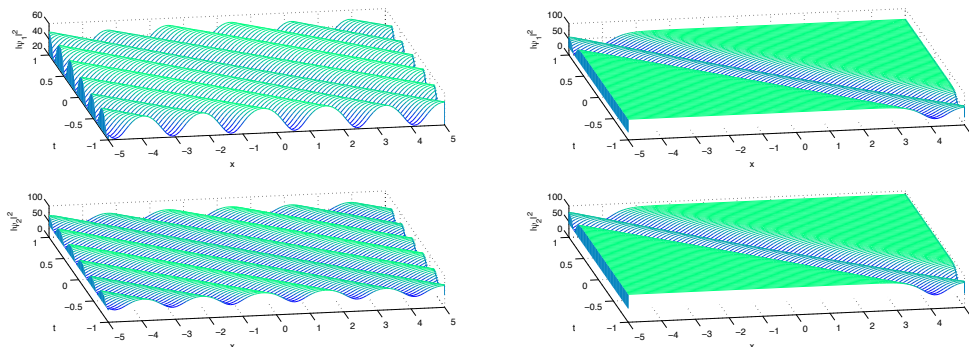


FIGURE 11. Solution (3.3) to the 2-NLS $^{\hat{s}}$ equation with $\hat{s} = (1, -1)$ on a hyperelliptic curve of genus 2 with branch points $-2, -1, 0, \epsilon, 2, 2 + \epsilon$ and $a_1 = (-1.9)^{(1)}$, $a_2 = (-1.8)^{(1)}$ and $a_3 = (-1.1)^{(1)}$ for $\epsilon = 1$ on the left and $\epsilon = 10^{-10}$, the almost solitonic limit, on the right.

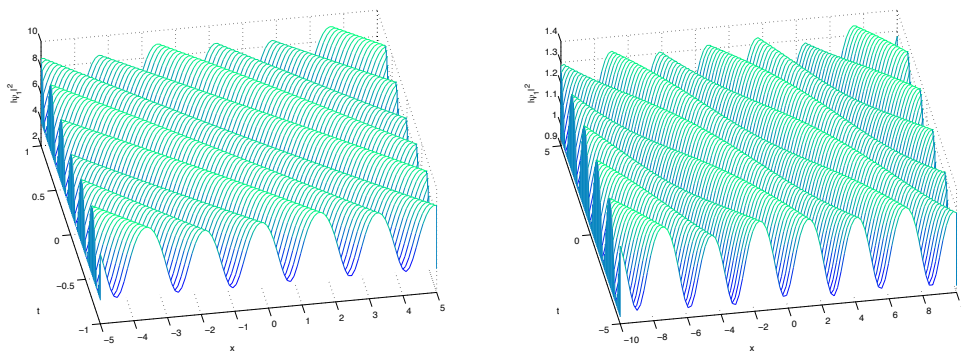


FIGURE 12. Solution to the 4-NLS $^{\hat{s}}$ equation on a hyperelliptic curve of genus 4 with branch points $-4, -3, -2, -2 + \epsilon, 0, \epsilon, 2, 2 + \epsilon, 4, 4 + \epsilon$ and $\epsilon = 1$ for $a_1 = (-3.9)^{(1)}$, $a_2 = (-3.7)^{(1)}$, $a_3 = (-3.5)^{(1)}$, $a_4 = (-3.3)^{(1)}$ and $a_5 = (-3.1)^{(1)}$, which leads to $\hat{s} = (1, -1, 1, -1)$, on the left, and for $a_1 = (-3.9)^{(1)}$, $a_2 = (-3.7)^{(1)}$, $a_3 = (-3.5)^{(1)}$, $a_4 = (-3.1)^{(1)}$ and $a_5 = (-3.3)^{(1)}$, which leads to $\hat{s} = (-1, 1, -1, -1)$ on the right.

The almost solitonic limit $\epsilon = 10^{-10}$ produces well known solitonic patterns as shown for instance for the DS equation in the previous subsection.

Hyperelliptic solutions to the n -NLS $^{\hat{s}}$ equation with all signs \hat{s}_j satisfying $\hat{s}_j = 1$, can be constructed on a curve without real branch points. To obtain smooth solutions, we use

$\mathbf{d} = 0$. A solution of the 2-NLS \hat{s} equation is studied on the curve of genus 2 with the branch points $-2 \pm i, -1 \pm i, 1 \pm i$ in Fig. 13.

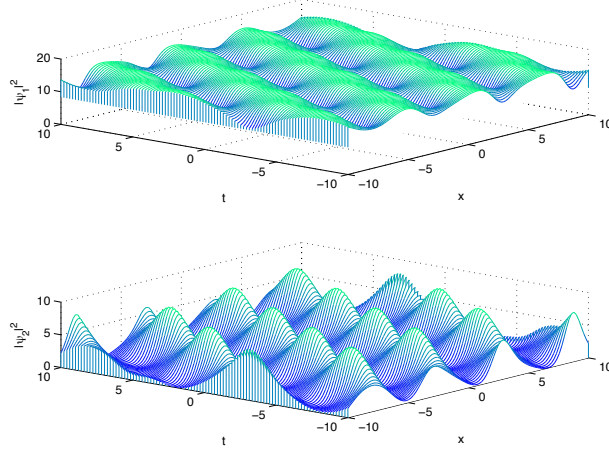


FIGURE 13. Solution to the 2-NLS \hat{s} equation with $\hat{s} = (1, 1)$ on a hyperelliptic curve of genus 2 with branch points $-2 \pm i, -1 \pm i, 1 \pm i$ and $a_1 = (-1.9)^{(1)}$, $a_2 = (-1.8)^{(2)}$ and $a_3 = (-1.1)^{(1)}$.

A typical example for a hyperelliptic 4-NLS \hat{s} solution with $\hat{s} = (1, 1, 1, 1)$ can be obtained on a curve of genus 4 with branch points $-2 \pm i, -1 \pm i, \pm i, 1 \pm i, 2 \pm i$, as shown in Fig. 14.

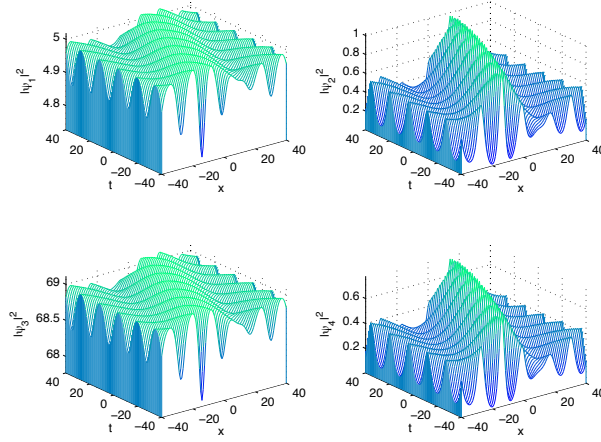


FIGURE 14. Solution to the 4-NLS \hat{s} equation with $\hat{s} = (1, 1, 1, 1)$ on a hyperelliptic curve of genus 4 with branch points $-2 \pm i, -1 \pm i, \pm i, 1 \pm i, 2 \pm i$ and $a_1 = (-3.9)^{(1)}$, $a_2 = (-3.7)^{(2)}$, $a_3 = (-3.5)^{(1)}$, $a_4 = (-3.3)^{(2)}$ and $a_5 = (-3.1)^{(1)}$.

4. GENERAL REAL ALGEBRAIC CURVES

The quantities entering theta-functional solutions of the DS and n -NLS^s equations are related to compact Riemann surfaces. Since all compact Riemann surfaces can be defined via compactified non-singular algebraic curves, convenient computational approaches as [6, 7] and [16] are based on algebraic curves: differentials, homology basis and periods of the Riemann surface can be obtained in an algorithmic way. We refer the reader to the cited literature for details. The identification of the sheets of the covering defined by the algebraic curve (1.1) via the projection map $(x, y) \mapsto x$, is done, as in the hyperelliptic case, by analytic continuation of the roots y_i , $i = 1, \dots, N$ for some non-critical point x_b on the x -sphere, along a set of contours specified in [16]. In the context of real algebraic curves for which solutions of n -NLS^s and DS are discussed here, an additional problem is to establish the action of the anti-holomorphic involution τ on points on different sheets. A typical problem is to find points $a \in \mathcal{R}_g$ and $b \in \mathcal{R}_g$ with the same projection onto the x -sphere such that $\tau a = b$; here τ is defined via $\tau a = (\bar{x}(a), \bar{y}(a))$. To this end, the roots y_i , $i = 1, \dots, N$, identified at $x = x_b$, are analytically continued to the points projecting to $x(a)$ on the x -sphere. It is then established which pairs of points in the different sheets satisfy $\tau a = b$.

In contrast to the hyperelliptic curves of the previous section, it is not possible for general curves to introduce a priori a basis of the homology. Thus the cited codes use an algorithm by Tretkoff and Tretkoff [28] which produces a homology basis for a given branching structure of the covering which is in general not adapted to possible automorphisms of the curve. In the context of theta-functional solutions to integrable PDEs one is often interested in real curves. As discussed in [19], the Vinnikov basis (i.e., the canonical homology basis which satisfies (2.19)) is convenient in this context. Since solutions and smoothness conditions for n -NLS^s and DS equations are formulated in this basis, a symplectic transformation relating the computed basis to the Vinnikov basis needs to be worked out. This transformation is discussed in the present section and will be applied to examples of real algebraic curves.

4.1. Symplectic transformation. Let \mathcal{R}_g be a real compact Riemann surface of genus g and τ an anti-holomorphic involution defined on it. Let (ν_1, \dots, ν_g) be a basis of holomorphic differentials such that

$$(4.1) \quad \overline{\tau^* \nu_j} = \nu_j, \quad j = 1, \dots, g,$$

where τ^* is the action of τ lifted to the space of holomorphic differentials: $\tau^* \omega(p) = \omega(\tau p)$ for any $p \in \mathcal{R}_g$. For an arbitrary canonical homology basis $(\mathcal{A}, \mathcal{B})$, let us denote by $P_{\mathcal{A}}$ and $P_{\mathcal{B}}$ the matrices of \mathcal{A} and \mathcal{B} -periods of the differentials ν_j :

$$(4.2) \quad (P_{\mathcal{A}})_{ij} = \int_{\mathcal{A}_i} \nu_j, \quad (P_{\mathcal{B}})_{ij} = \int_{\mathcal{B}_i} \nu_j, \quad i, j = 1, \dots, g.$$

In what follows $(\mathcal{A}, \mathcal{B})$ denotes the Vinnikov basis. From (4.1) and (2.19) we deduce the action of the complex conjugation on the matrices $P_{\mathcal{A}}$ and $P_{\mathcal{B}}$:

$$(4.3) \quad (P_{\mathcal{A}})_{ij} \in \mathbb{R},$$

$$(4.4) \quad \overline{P_{\mathcal{B}}} = -P_{\mathcal{B}} + \mathbb{H}P_{\mathcal{A}}.$$

Denote by $(\tilde{\mathcal{A}}, \tilde{\mathcal{B}})$ the homology basis on \mathcal{R}_g produced by the Tretkoff-Tretkoff algorithm. From the symplectic transformation (2.5) we obtain the following transformation

law between the matrices $P_{\tilde{\mathcal{A}}}, P_{\tilde{\mathcal{B}}}$ and $P_{\mathcal{A}}, P_{\mathcal{B}}$ defined in (4.2):

$$(4.5) \quad \begin{pmatrix} A & B \\ C & D \end{pmatrix} \begin{pmatrix} P_{\tilde{\mathcal{A}}} \\ P_{\tilde{\mathcal{B}}} \end{pmatrix} = \begin{pmatrix} P_{\mathcal{A}} \\ P_{\mathcal{B}} \end{pmatrix}.$$

Therefore, by (4.3) one gets

$$(4.6) \quad A \operatorname{Re}(P_{\tilde{\mathcal{A}}}) + B \operatorname{Re}(P_{\tilde{\mathcal{B}}}) = P_{\mathcal{A}}$$

$$(4.7) \quad A \operatorname{Im}(P_{\tilde{\mathcal{A}}}) + B \operatorname{Im}(P_{\tilde{\mathcal{B}}}) = 0,$$

and by (4.4)

$$(4.8) \quad C \operatorname{Re}(P_{\tilde{\mathcal{A}}}) + D \operatorname{Re}(P_{\tilde{\mathcal{B}}}) = \frac{1}{2} \mathbb{H} P_{\mathcal{A}}$$

$$(4.9) \quad C \operatorname{Im}(P_{\tilde{\mathcal{A}}}) + D \operatorname{Im}(P_{\tilde{\mathcal{B}}}) = \operatorname{Im}(P_{\mathcal{B}}).$$

According to (4.6), the matrix $A \operatorname{Re}(P_{\tilde{\mathcal{A}}}) + B \operatorname{Re}(P_{\tilde{\mathcal{B}}})$ is invertible, since the matrix $P_{\mathcal{A}}$ of \mathcal{A} -periods of a basis of holomorphic differentials is always invertible (see, for instance, [3]). Moreover, it is well known that the Riemann matrix $\mathbb{B} = 2i\pi P_{\mathcal{B}}(P_{\mathcal{A}})^{-1}$ has a (negative) definite real part, which is equal to $-2\pi \operatorname{Im}(P_{\mathcal{B}}) \operatorname{Im}((P_{\mathcal{A}})^{-1})$ for the real matrix $P_{\mathcal{A}}$ here. Then, by (4.9) the matrix $C \operatorname{Im}(P_{\tilde{\mathcal{A}}}) + D \operatorname{Im}(P_{\tilde{\mathcal{B}}})$ is also invertible.

Lemma 4.1. *The matrices $A, B, C, D \in \mathcal{M}_g(\mathbb{Z})$ solving (4.6)-(4.9) satisfy:*

$$(4.10) \quad A^t = \operatorname{Im}(P_{\tilde{\mathcal{B}}}) [C \operatorname{Im}(P_{\tilde{\mathcal{A}}}) + D \operatorname{Im}(P_{\tilde{\mathcal{B}}})]^{-1}$$

$$(4.11) \quad B^t = -\operatorname{Im}(P_{\tilde{\mathcal{A}}}) [C \operatorname{Im}(P_{\tilde{\mathcal{A}}}) + D \operatorname{Im}(P_{\tilde{\mathcal{B}}})]^{-1}$$

$$(4.12) \quad C^t = \frac{1}{2} A^t \mathbb{H} - \operatorname{Re}(P_{\tilde{\mathcal{B}}}) [A \operatorname{Re}(P_{\tilde{\mathcal{A}}}) + B \operatorname{Re}(P_{\tilde{\mathcal{B}}})]^{-1}$$

$$(4.13) \quad D^t = \frac{1}{2} B^t \mathbb{H} + \operatorname{Re}(P_{\tilde{\mathcal{A}}}) [A \operatorname{Re}(P_{\tilde{\mathcal{A}}}) + B \operatorname{Re}(P_{\tilde{\mathcal{B}}})]^{-1}.$$

Proof. Recall that symplectic matrices $M = \begin{pmatrix} A & B \\ C & D \end{pmatrix} \in Sp(2g, \mathbb{Z})$ are characterized by

$$(4.14) \quad A^t D - C^t B = \mathbb{I}_g,$$

$$(4.15) \quad A^t C = C^t A,$$

$$(4.16) \quad D^t B = B^t D.$$

Multiplying equality (4.7) from the left by the matrix C^t , we deduce from (4.14) and (4.15) that:

$$\begin{aligned} C^t A \operatorname{Im}(P_{\tilde{\mathcal{A}}}) + C^t B \operatorname{Im}(P_{\tilde{\mathcal{B}}}) &= 0 \\ C^t A \operatorname{Im}(P_{\tilde{\mathcal{A}}}) + (A^t D - \mathbb{I}_g) \operatorname{Im}(P_{\tilde{\mathcal{B}}}) &= 0 \\ A^t C \operatorname{Im}(P_{\tilde{\mathcal{A}}}) + A^t D \operatorname{Im}(P_{\tilde{\mathcal{B}}}) &= \operatorname{Im}(P_{\tilde{\mathcal{B}}}), \end{aligned}$$

which leads to (4.10). Equality (4.11) can be checked analogously with (4.14) and (4.16). To prove (4.12), multiply equality (4.8) from the left by the matrix A^t . Using (4.14) and

(4.15) one gets:

$$\begin{aligned} A^t C \operatorname{Re}(P_{\tilde{\mathcal{A}}}) + A^t D \operatorname{Re}(P_{\tilde{\mathcal{B}}}) &= \frac{1}{2} A^t \mathbb{H} P_{\mathcal{A}} \\ C^t A \operatorname{Re}(P_{\tilde{\mathcal{A}}}) + (\mathbb{I}_g + C^t B) \operatorname{Re}(P_{\tilde{\mathcal{B}}}) &= \frac{1}{2} A^t \mathbb{H} P_{\mathcal{A}} \\ C^t (A \operatorname{Re}(P_{\tilde{\mathcal{A}}}) + B \operatorname{Re}(P_{\tilde{\mathcal{B}}})) &= \frac{1}{2} A^t \mathbb{H} P_{\mathcal{A}} - \operatorname{Re}(P_{\tilde{\mathcal{B}}}), \end{aligned}$$

which by (4.6) leads to (4.12). Identity (4.13) can be proved analogously. \square

Remark 4.1. Lemma 4.1 implies that it is sufficient to know the matrices A and B (or C and D) to determine the symplectic matrix in (4.5). In practice, this means that a convenient ansatz for one of the matrices has to be found. The others then follow from the relations in Lemma 4.1.

Thus to construct these matrices one first checks which of the matrices $\operatorname{Re}(P_{\tilde{\mathcal{A}}})$, $\operatorname{Re}(P_{\tilde{\mathcal{B}}})$, $\operatorname{Im}(P_{\tilde{\mathcal{A}}})$, $\operatorname{Im}(P_{\tilde{\mathcal{B}}})$ are invertible. This way a matrix can be identified (e.g. A) in terms of which the others can be expressed. The task is thus reduced to provide an ansatz for this matrix such that the others will have entire components. We illustrate this approach at the example of the Trott curve below.

Proposition 4.1. *Let $(\tilde{\mathcal{A}}, \tilde{\mathcal{B}})$ be the canonical homology basis obtained with the Tretkoff-Trethoff algorithm; we denote with a tilde the quantities expressed in this basis. Under the change of homology basis (2.5), solutions of n -NLS^s and DS equations given in (2.22) and (2.27), respectively, which are expressed in the basis satisfying (2.19), transform as follows: the vector \mathbf{d} appearing in the solutions becomes $(2i\pi)^{-1} \tilde{\mathbb{K}}^t \mathbf{d}$ where $\tilde{\mathbb{K}} = 2i\pi A + B \tilde{\mathbb{B}}$, and the theta function $\Theta = \Theta_{\mathbb{B}}$ with zero characteristic, transforms to the theta function $\Theta_{\tilde{\mathbb{B}}}[\tilde{\delta}]$ with characteristic $\tilde{\delta} = [\tilde{\delta}_1, \tilde{\delta}_2]$ given by*

$$(4.17) \quad \tilde{\delta}_1 = \frac{1}{4} \operatorname{diag} \left(B^t \mathbb{H} B - 2 \operatorname{Re}(P_{\tilde{\mathcal{A}}}) \tilde{\mathbb{M}}^{-1} \operatorname{Im}(P_{\tilde{\mathcal{A}}}^t) \right),$$

$$(4.18) \quad \tilde{\delta}_2 = \frac{1}{4} \operatorname{diag} \left(A^t \mathbb{H} A - 2 \operatorname{Re}(P_{\tilde{\mathcal{B}}}) \tilde{\mathbb{M}}^{-1} \operatorname{Im}(P_{\tilde{\mathcal{B}}}^t) \right),$$

where

$$(4.19) \quad \tilde{\mathbb{M}} = \operatorname{Im}(P_{\tilde{\mathcal{B}}}^t) \operatorname{Re}(P_{\tilde{\mathcal{A}}}) - \operatorname{Im}(P_{\tilde{\mathcal{A}}}^t) \operatorname{Re}(P_{\tilde{\mathcal{B}}}).$$

Moreover, the real constant h appearing in (2.28) and (2.31) becomes $h + \tilde{h}$ where $\operatorname{Im}(\tilde{h})$ is given by

$$(4.20) \quad \operatorname{Im}(\tilde{h}) = \frac{1}{2} \ln \left\{ \left| \frac{\Theta_{\tilde{\mathbb{B}}}[\tilde{\delta}](\tilde{\mathbf{Z}} + \tilde{\mathbf{r}})}{\Theta_{\tilde{\mathbb{B}}}[\tilde{\delta}](\tilde{\mathbf{Z}} - \tilde{\mathbf{r}})} \right| \right\} - \operatorname{Im}(\tilde{G}_3),$$

with $\tilde{\mathbf{Z}} = i(\tilde{\mathbf{W}}_a - \tilde{\mathbf{W}}_b)$, and the vectors \mathbf{N}, \mathbf{M} defined in (2.20) become $A^t \mathbf{N} + C^t \mathbf{M}$ and $B^t \mathbf{N} + D^t \mathbf{M}$ respectively.

Proof. Under the change of the canonical homology basis (2.5), the vector $\omega = (\omega_1, \dots, \omega_g)^t$ of normalized holomorphic differentials transforms as

$$(4.21) \quad \omega = 2i\pi (\tilde{\mathbb{K}}^t)^{-1} \tilde{\omega},$$

where $\tilde{\mathbb{K}} = 2i\pi A + B \tilde{\mathbb{B}}$. According to the transformation law (2.6) of theta functions, it can be checked after straightforward calculations, that under this change of homology

basis, quantities (2.15)-(2.17) transform as:

$$(4.22) \quad q_2(a, b) = \tilde{q}_2(a, b) \exp \left\{ -\tilde{\mathbf{r}}^t (\tilde{\mathbb{K}}^t)^{-1} B \tilde{\mathbf{r}} \right\},$$

$$(4.23) \quad q_1(a, b) = \tilde{q}_1(a, b) + \frac{1}{2} \tilde{\mathbf{V}}_a^t (\tilde{\mathbb{K}}^t)^{-1} B \tilde{\mathbf{V}}_b,$$

$$(4.24) \quad K_1(a, b) = \tilde{K}_1(a, b) + \frac{1}{2} \left(\tilde{\mathbf{V}}_a^t (\tilde{\mathbb{K}}^t)^{-1} B \tilde{\mathbf{r}} + \tilde{\mathbf{r}}^t (\tilde{\mathbb{K}}^t)^{-1} B \tilde{\mathbf{V}}_a \right),$$

$$(4.25) \quad K_2(a, b) = \tilde{K}_2(a, b) - \frac{1}{2} \left(\tilde{\mathbf{W}}_a^t (\tilde{\mathbb{K}}^t)^{-1} B \tilde{\mathbf{r}} + \tilde{\mathbf{r}}^t (\tilde{\mathbb{K}}^t)^{-1} B \tilde{\mathbf{W}}_a \right) - \tilde{\mathbf{V}}_a^t (\tilde{\mathbb{K}}^t)^{-1} B \tilde{\mathbf{V}}_a.$$

We deduce that solutions of the n -NLS^s and DS equations given in (2.22) and (2.27), respectively, transform as follows: the vector \mathbf{d} becomes $(2i\pi)^{-1} \tilde{\mathbb{K}}^t \mathbf{d}$, and the theta function $\Theta = \Theta_{\mathbb{B}}$ with zero characteristic, transforms to the theta function $\Theta_{\tilde{\mathbb{B}}}[\tilde{\delta}]$ with characteristic $\tilde{\delta}$. To compute the vectors of the characteristic $\tilde{\delta}$ we consider the inversion of the symplectic matrix in (2.5) which leads to

$$\begin{pmatrix} \tilde{\mathcal{A}} \\ \tilde{\mathcal{B}} \end{pmatrix} = \begin{pmatrix} D^t & -B^t \\ -C^t & A^t \end{pmatrix} \begin{pmatrix} \mathcal{A} \\ \mathcal{B} \end{pmatrix}.$$

Since the characteristic used in [19] to construct solutions (2.22), (2.27) of n -NLS^s and DS is zero, we get with (2.9)

$$\begin{pmatrix} \tilde{\delta}_1 \\ \tilde{\delta}_2 \end{pmatrix} = \frac{1}{2} \text{Diag} \begin{pmatrix} D^t B \\ C^t A \end{pmatrix}$$

(note that $D^t B$ and $C^t A$ are symmetric matrices). Substituting (4.10) and (4.11) in (4.12) (resp. (4.13)), it can be checked that

$$\begin{aligned} C^t A &= \frac{1}{2} \left(A^t \mathbb{H} A - 2 \text{Re} (P_{\tilde{\mathcal{B}}}^t) \tilde{\mathbb{M}}^{-1} \text{Im} (P_{\tilde{\mathcal{B}}}^t) \right), \\ D^t B &= \frac{1}{2} \left(B^t \mathbb{H} B - 2 \text{Re} (P_{\tilde{\mathcal{A}}}^t) \tilde{\mathbb{M}}^{-1} \text{Im} (P_{\tilde{\mathcal{A}}}^t) \right), \end{aligned}$$

with

$$\tilde{\mathbb{M}} = \text{Im} (P_{\tilde{\mathcal{B}}}^t) \text{Re} (P_{\tilde{\mathcal{A}}}^t) - \text{Im} (P_{\tilde{\mathcal{A}}}^t) \text{Re} (P_{\tilde{\mathcal{B}}}^t).$$

Moreover, the real constant h appearing in the solutions (2.27)-(2.28) of the Davey-Stewartson equations becomes $h + \tilde{h}$, where \tilde{h} is given by

$$(4.26) \quad \tilde{h} = -\tilde{\mathbf{V}}_a^t (\tilde{\mathbb{K}}^t)^{-1} B \tilde{\mathbf{V}}_a - \tilde{\mathbf{V}}_b^t (\tilde{\mathbb{K}}^t)^{-1} B \tilde{\mathbf{V}}_b.$$

Notice that the construction of the solutions (2.27) given in [19] allows to express the imaginary part of the constant \tilde{h} (4.26) in terms of the characteristic $\tilde{\delta}$. Namely, since the reality condition

$$(4.27) \quad \psi^* = \rho \bar{\psi}$$

is satisfied for the Vinnikov basis, where the function $\psi^*(\xi, \eta, t)$ reads

$$(4.28) \quad \psi^*(\xi, \eta, t) = -\kappa_1 \kappa_2 \frac{q_2(a, b)}{A} \frac{\Theta(\mathbf{Z} - \mathbf{d} - \mathbf{r})}{\Theta(\mathbf{Z} - \mathbf{d})} \exp \left\{ i \left(G_1 \xi + G_2 \eta - G_3 \frac{t}{2} \right) \right\},$$

it also holds for the computed basis. Therefore, putting $\xi = \eta = 0$, $t = 2$, $\mathbf{d} = 0$, and taking the modulus of each term in (4.27) expressed in the computed basis, one gets:

$$\left| \frac{\Theta_{\mathbb{B}}[\tilde{\delta}](\tilde{\mathbf{Z}} - \tilde{\mathbf{r}})}{\Theta_{\mathbb{B}}[\tilde{\delta}](\tilde{\mathbf{Z}})} \exp\{-i(\tilde{G}_3 + \tilde{h})\} \right| = \left| \frac{\Theta_{\mathbb{B}}[\tilde{\delta}](\tilde{\mathbf{Z}} + \tilde{\mathbf{r}})}{\Theta_{\mathbb{B}}[\tilde{\delta}](\tilde{\mathbf{Z}})} \exp\{i(\tilde{G}_3 + \tilde{h})\} \right|$$

where $\tilde{\mathbf{Z}} = i(\tilde{\mathbf{W}}_a - \tilde{\mathbf{W}}_b)$. We deduce that

$$(4.29) \quad \text{Im}(\tilde{h}) = \frac{1}{2} \ln \left\{ \left| \frac{\Theta_{\mathbb{B}}[\tilde{\delta}](\tilde{\mathbf{Z}} + \tilde{\mathbf{r}})}{\Theta_{\mathbb{B}}[\tilde{\delta}](\tilde{\mathbf{Z}} - \tilde{\mathbf{r}})} \right| \right\} - \text{Im}(\tilde{G}_3).$$

□

Remark 4.2. *In the case where the spectral curve is an M-curve, i.e. $\mathbb{H} = 0$, the vectors of characteristic (4.17) and (4.18) do not depend explicitly on the symplectic matrix appearing in the change of homology basis and are uniquely defined by:*

$$(4.30) \quad \tilde{\delta}_1 = \frac{1}{2} \text{diag} \left(\text{Re}(P_{\tilde{\mathcal{A}}}) \left[\text{Im}(P_{\tilde{\mathcal{B}}}^t) \text{Re}(P_{\tilde{\mathcal{A}}}) - \text{Im}(P_{\tilde{\mathcal{A}}}^t) \text{Re}(P_{\tilde{\mathcal{B}}}) \right]^{-1} \text{Im}(P_{\tilde{\mathcal{A}}}^t) \right),$$

$$(4.31) \quad \tilde{\delta}_2 = \frac{1}{2} \text{diag} \left(\text{Re}(P_{\tilde{\mathcal{B}}}) \left[\text{Im}(P_{\tilde{\mathcal{B}}}^t) \text{Re}(P_{\tilde{\mathcal{A}}}) - \text{Im}(P_{\tilde{\mathcal{A}}}^t) \text{Re}(P_{\tilde{\mathcal{B}}}) \right]^{-1} \text{Im}(P_{\tilde{\mathcal{B}}}^t) \right).$$

It would be possible to compute the theta-functional solutions in the Vinnikov basis once the symplectic transformation between this basis and the basis determined by the code is known. However, since this symplectic transformation is not unique, the found Vinnikov basis leads in general to a Riemann matrix for which the theta series converges only slowly, i.e., the value N_θ in (3.2) has to be chosen very large. To avoid this problem, we compute the theta function always in the typically more convenient Tretkoff-Tretkoff basis with the characteristic of the theta functions given by (4.17)-(4.19).

4.2. Trott curve. The Trott curve [29] given by the algebraic equation

$$(4.32) \quad 144(x^4 + y^4) - 225(x^2 + y^2) + 350x^2y^2 + 81 = 0$$

is an M-curve with respect to the anti-holomorphic involution τ defined by $\tau(x, y) = (\bar{x}, \bar{y})$, and is of genus 3. Moreover, this curve has real branch points only (and 28 real bitangents, namely, tangents to the curve in two places). Our computed matrices of $\tilde{\mathcal{A}}$ and $\tilde{\mathcal{B}}$ -periods read²

$$P_{\tilde{\mathcal{A}}} = \begin{pmatrix} 0.0235i & 0.0138i & 0.0138i \\ 0 & 0.0277i & 0 \\ -0.0315 & 0 & 0.0250 \end{pmatrix},$$

$$P_{\tilde{\mathcal{B}}} = \begin{pmatrix} -0.0315 + 0.0235i & 0.0138i & -0.0250 + 0.0138i \\ 0 & -0.025 + 0.0277i & 0.0250 \\ -0.0235i & 0.0138i & 0.0138i \end{pmatrix}.$$

The Trott curve being an M-curve, the vectors of the characteristic $\tilde{\delta}$ satisfy (4.30) and (4.31), which leads to $\tilde{\delta} = \frac{1}{2} \begin{bmatrix} 0 & 0 & 0 \\ 1 & 1 & 0 \end{bmatrix}^t$.

²For the ease of representation we only give 4 digits here, though at least 12 digits are known for these quantities.

A possible choice of a symplectic transformation bringing the computed basis to the Vinnikov basis is:

$$A = \begin{pmatrix} 1 & 0 & 0 \\ 0 & 1 & 0 \\ 0 & 0 & 1 \end{pmatrix}, \quad B = \begin{pmatrix} -1 & 0 & 0 \\ 0 & -1 & 0 \\ 0 & 0 & 0 \end{pmatrix}, \quad C = \begin{pmatrix} 1 & 0 & 0 \\ 0 & 1 & 0 \\ 0 & 0 & 0 \end{pmatrix}, \quad D = \begin{pmatrix} 0 & 0 & 0 \\ 0 & 0 & 0 \\ 0 & 0 & 1 \end{pmatrix}.$$

Note that the matrices A, B, C, D are not unique since the action (2.19) of the anti-holomorphic involution on the basic cycles allows for permutations of \mathcal{A}_j -cycles for instance. These matrices can be computed as follows. Since the Trott curve is an M-curve, one has $\mathbb{H} = 0$. Moreover, the matrix $\text{Im}(P_{\tilde{\mathcal{B}}})$ being invertible here, by (4.7) one gets:

$$(4.33) \quad B = -A \text{Im}(P_{\tilde{\mathcal{A}}}) (\text{Im}(P_{\tilde{\mathcal{B}}}))^{-1}.$$

With (4.14) and (4.15) it follows that

$$(4.34) \quad A^t (D + C \text{Im}(P_{\tilde{\mathcal{A}}}) (\text{Im}(P_{\tilde{\mathcal{B}}}))^{-1}) = \mathbb{I}_3.$$

The computed matrix $\text{Im}(P_{\tilde{\mathcal{A}}}) (\text{Im}(P_{\tilde{\mathcal{B}}}))^{-1}$ being (within numerical precision) equal to

$$\text{Im}(P_{\tilde{\mathcal{A}}}) (\text{Im}(P_{\tilde{\mathcal{B}}}))^{-1} = \begin{pmatrix} -1 & 0 & 0 \\ 0 & -1 & 0 \\ 0 & 0 & 0 \end{pmatrix},$$

and with $C, D \in \mathcal{M}_3(\mathbb{Z})$, we get from (4.34) that $\det A = 1$. Since $A \in \mathcal{M}_3(\mathbb{Z})$, the condition $\det A = 1$ implies $A \in \text{Gl}_3(\mathbb{Z})$. For any $A \in \text{Gl}_3(\mathbb{Z})$, one can see from (4.33), (4.12) and (4.13) that $B, C, D \in \mathcal{M}_3(\mathbb{Z})$, and therefore that the matrices A, B, C, D give a solution of (4.6)-(4.9). The choice $A = \mathbb{I}_3$ leads to the above matrices.

The Trott curve has real fibers and can thus be used to construct solutions to the 3-NLS equation via the projection map $f : (x, y) \mapsto x$, which is a real meromorphic function of degree 4 on the curve. We consider the points on the curve stable with respect to τ and projecting to the point with $x = 0.1$ in the x -sphere, and choose $\mathbf{d} = 0$. The corresponding solution to the 3-NLS equation can be seen in Fig. 15.

A solution to the DS1⁺ equation on this curve can be constructed for points a and b stable with respect to the involution τ . The solution for $a = (-0.2)^{(1)}$, $b = (0.2)^{(2)}$ and the choice $\mathbf{d} = 0$ can be seen in Fig. 16. Note that in accordance with Remark 2.1, one would obtain a solution of DS1⁻ for the choice $a = (-0.2)^{(1)}$ and $b = (0.2)^{(1)}$.

Similarly, a solution to the DS2⁺ equation can be obtained for points a and b subject to $\tau a = b$. For $a = (0.1 + i)^{(1)}$ and $b = (0.1 - i)^{(1)}$ we get Fig. 17.

4.3. Dividing curves without real branch point.

We consider the curve given by the equation

$$(4.35) \quad 30x^4 - 61x^3y + 41y^2x^2 - 43x^2 - 11y^3x + 42xy + y^4 - 11y^2 + 9 = 0$$

which was studied in [10] and [30]. It is a genus 3 curve, dividing with respect to the anti-holomorphic involution τ , without real branch point. This curve admits two real ovals. In this case the matrix \mathbb{H} has the form

$$\mathbb{H} = \begin{pmatrix} 0 & 1 & 0 \\ 1 & 0 & 0 \\ 0 & 0 & 0 \end{pmatrix}.$$

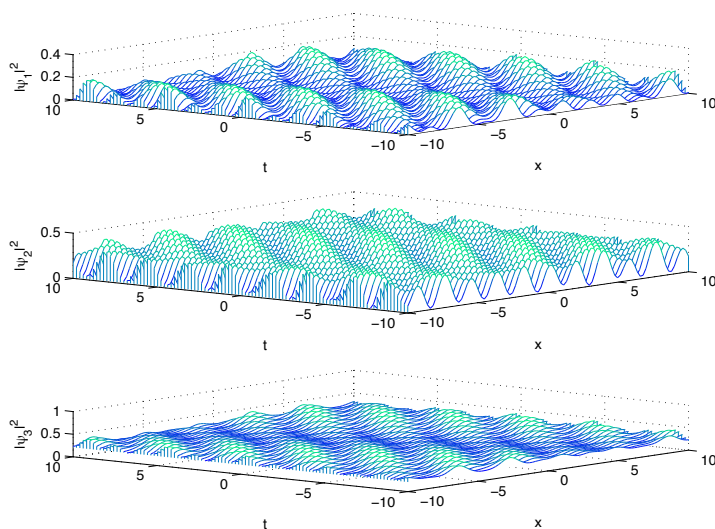


FIGURE 15. *Solution (2.22) to the 3-NLS^s equation on the Trott curve for the points with $x = 0.1$ on the x -sphere. The sheets are identified at the points projecting to $x = -1.0129, (0.9582i, -0.9582i, 0.1146i, -0.1146i)$. The vector of signs equals $s = (1, -1, -1)$ from top to bottom.*

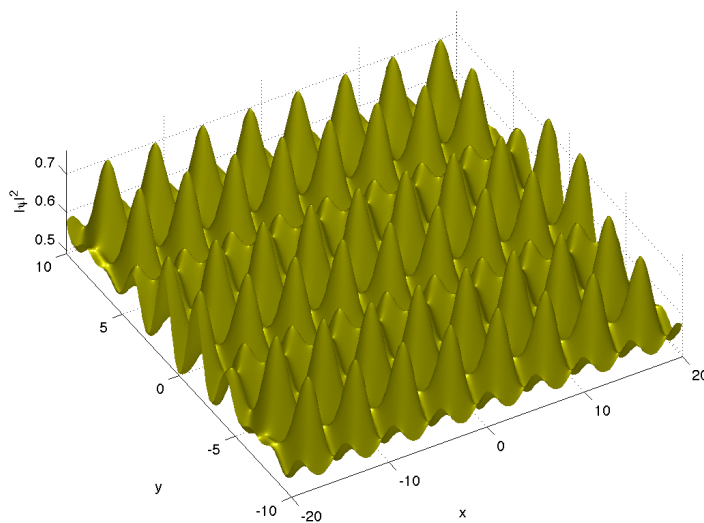


FIGURE 16. *Solution to the DS1⁺ equation on the Trott curve for the points $a = (-0.2)^{(1)}$ and $b = (0.2)^{(2)}$ at $t = 0$.*

The period matrices computed by the code read

$$P_{\tilde{A}} = \begin{pmatrix} -0.2721 - 0.0977i & -0.3193 + 0.1914i & -1.0668 + 0.4293i \\ 0.2721 + 0.0977i & -0.3193 - 0.3341i & -1.0668 - 0.4316i \\ 0.2721 - 0.0977i & 0.4676 - 0.3341i & 0.7992 - 0.4316i \end{pmatrix},$$

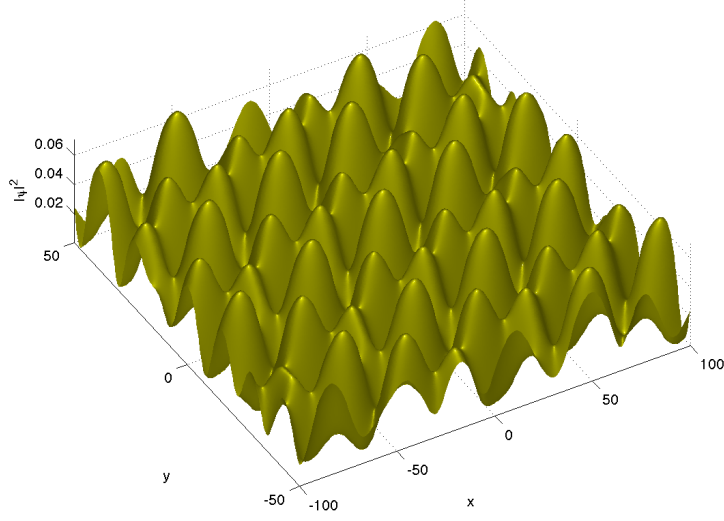


FIGURE 17. Solution to the $DS2^+$ equation on the Trott curve for the points $a = (0.1 + i)^{(1)}$ and $b = (0.1 - i)^{(1)}$ at $t = 0$.

$$P_{\tilde{B}} = \begin{pmatrix} -0.2721 - 0.2932i & -0.3193 + 0.3341i & -1.0668 + 0.4316i \\ 0.2721 + 0.2932i & -0.3193 - 0.7169i & -1.0668 - 1.2903i \\ 0.2721 - 0.0977i & 0.4676 + 0.1914i & 0.7992 + 0.4293i \end{pmatrix}.$$

After some calculations, one finds that the following matrices A, B, C, D provide a solution of (4.6)-(4.9):

$$A = \begin{pmatrix} -1 & 2 & -1 \\ 2 & -1 & 0 \\ 0 & 2 & -1 \end{pmatrix}, B = \begin{pmatrix} 1 & 0 & 1 \\ 0 & 1 & 0 \\ 1 & 0 & 0 \end{pmatrix}, C = \begin{pmatrix} 1 & -1 & -1 \\ -1 & 1 & -1 \\ 0 & 0 & 1 \end{pmatrix}, D = \begin{pmatrix} 0 & 1 & 1 \\ 1 & 0 & 1 \\ 0 & 0 & -1 \end{pmatrix}.$$

From (4.17) and (4.18) one gets for the characteristic: $\tilde{\delta} = \frac{1}{2} \begin{bmatrix} 0 & 0 & 1 \\ 1 & 1 & 0 \end{bmatrix}^t$.

The curve (4.35) has real fibers and can thus be used to construct solutions to the focusing 3-NLS equation. We consider the points on the curve with $x = 2.5$ and stable with respect to τ , and we choose $\mathbf{d} = 0$. The corresponding solution to the focusing 3-NLS equation can be seen in Fig. 18.

A solution to the $DS1^-$ equation can be constructed by choosing the points $a = (-4)^{(1)}$ and $b = (-3)^{(2)}$ see Fig. 19.

4.4. Fermat curve. The Fermat curves

$$(4.36) \quad y^n + x^n + 1 = 0, \quad n > 2, \quad n \text{ even},$$

are real curves without real oval with respect to τ . We consider here the curve with $n = 4$ that has genus 3. The matrix \mathbb{H} has the form

$$\mathbb{H} = \begin{pmatrix} 0 & 1 & 0 \\ 1 & 0 & 0 \\ 0 & 0 & 0 \end{pmatrix},$$

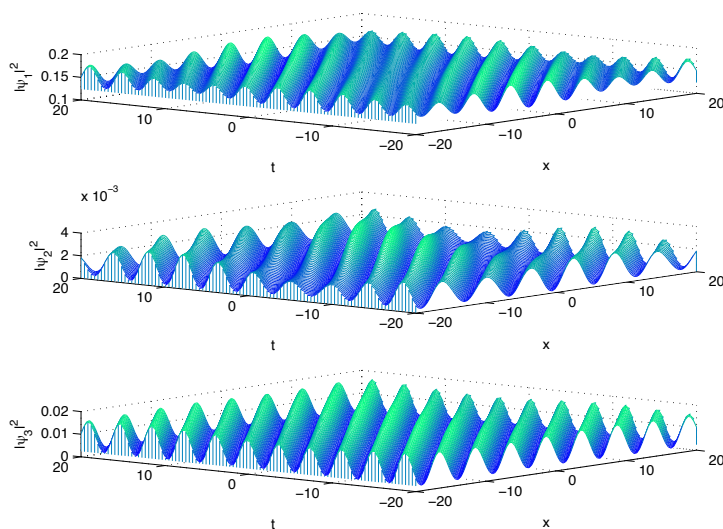


FIGURE 18. Solution to the 3-NLS^s equation on the dividing curve (4.35) of genus 3 for the points with $x = 2.5$ on the x -sphere. The sheets are identified at the fiber over $-2.1404 + 0.4404i$, $(-12.2492 + 2.0113i, -5.1634 + 1.3519i, -4.5915 + 0.9380i, -1.5405 + 0.5429i)$. The vector of signs is $s = (1, 1, 1)$.

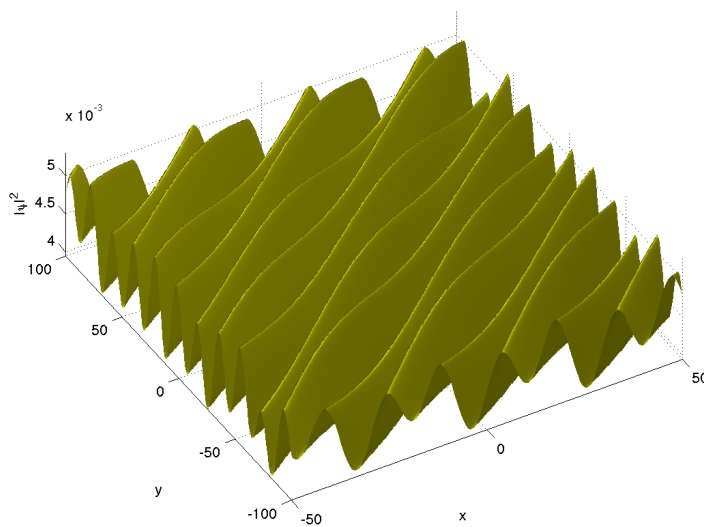


FIGURE 19. Solution to the DS1⁻ equation on the dividing curve (4.35) of genus 3 for the points $a = (-4)^{(1)}$ and $b = (-3)^{(2)}$ at $t = 0$.

and we find

$$P_{\tilde{\mathcal{A}}} = \begin{pmatrix} 0.9270 & -0.9270i & -0.9270i \\ 0 & 0 & -1.8541i \\ 0.9270i & -0.9270 & -0.9270i \end{pmatrix},$$

$$P_{\tilde{B}} = \begin{pmatrix} 0.9270 + 0.9270i & 0.9270 - 0.9270i & 0 \\ 0 & -0.9270 + 0.9270i & 0.9270 - 0.9270i \\ -0.9270 & -0.9270i & -0.9270i \end{pmatrix}.$$

The following matrices A, B, C, D provide a solution of (4.6)-(4.9):

$$A = \begin{pmatrix} 0 & 1 & 1 \\ 1 & 0 & 0 \\ 0 & 0 & 1 \end{pmatrix}, B = \begin{pmatrix} -1 & -2 & -1 \\ 0 & 0 & -1 \\ -1 & -1 & 0 \end{pmatrix}, C = \begin{pmatrix} 0 & 1 & 0 \\ 0 & 0 & 1 \\ 1 & -1 & 0 \end{pmatrix}, D = \begin{pmatrix} 0 & 0 & -1 \\ 0 & -1 & 0 \\ 0 & 0 & 1 \end{pmatrix},$$

which leads to the characteristic: $\tilde{\delta} = \frac{1}{2} \begin{bmatrix} 0 & 0 & 1 \\ 0 & 1 & 0 \end{bmatrix} t$.

To construct a solution of the $DS2^-$ equation on the Fermat curve, we choose the points $a = (-1.5 + i)^{(1)}$ and $b = (-1.5 - i)^{(3)}$. The resulting solution for the choice $\mathbf{d} = 0$ can be seen in Fig. 20.

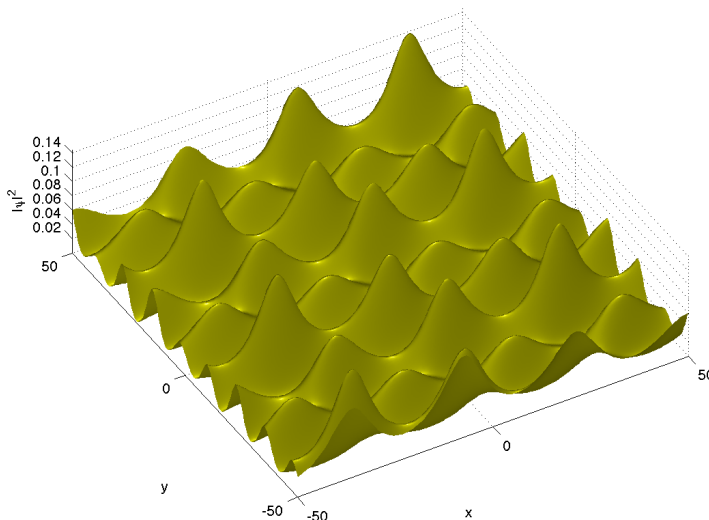


FIGURE 20. Solution to the $DS2^-$ equation on the Fermat curve (4.36) of genus 3 for the points $a = (-1.5 + i)^{(1)}$ and $b = (-1.5 - i)^{(3)}$ at $t = 0$.

5. CONCLUSION

In this paper we have presented the state of the art of the numerical evaluation of solutions to integrable equations in terms of multi-dimensional theta functions associated to real Riemann surfaces by using an approach via real algebraic curves. It was shown that real hyperelliptic curves parametrized by the branch points can be treated with machine precision for a wide range of the parameters. Even almost degenerate situations where the branch points coincide pairwise can be handled as long as at least one cut stays finite. This approach to real hyperelliptic curves [14, 15] is being generalized to arbitrary hyperelliptic curves.

As discussed in [16], the main difficulty for general algebraic curves is the correct numerical identification of the branch points. The case of degenerations for given branch points

has not yet been studied numerically, but is planned for the future. In what concerns the solutions (2.22) to n -NLS^s and similar solutions to the DS and the Kadomtsev-Petviashvili equations, the main problem in the context of real Riemann surfaces is to find the symplectic transformation leading to the homology basis introduced in [30], for which the solutions of the studied equations, with regularity conditions, can be conveniently formulated. This problem has been reduced to find a single $g \times g$ -matrix for given periods and real ovals, the latter encoded by the matrix \mathbb{H} . For M-curves, where the matrix \mathbb{H} vanishes, a general formula for the characteristic (4.17)-(4.19) could be given. In the general case, an algorithm along the lines indicated in the previous section to find the transformation will be based on a sufficiently general ansatz for one of the matrices entering the symplectic transformation which is the subject of future work.

REFERENCES

- [1] D. Anker, N.C. Freeman, *On the Soliton Solutions of the Davey-Stewartson Equation for Long Waves*, Proc. R. Soc. London A **360** 529 (1978).
- [2] E. Belokolos, A. Bobenko, V. Enolskii, A. Its, V. Matveev, *Algebro-geometric approach to nonlinear integrable equations*, Springer Series in nonlinear dynamics (1994).
- [3] A.I. Bobenko, C. Klein, (ed.), *Computational Approach to Riemann Surfaces*, Lect. Notes Math. **2013** (2011).
- [4] L.A. Bordag, A.I. Bobenko, *Periodic Multiphase Solutions of the Kadomtsev-Petviashvili-equation*, J. Phys. A: Math. and General **22**, p. 1259 (1989).
- [5] A. Davey and K. Stewartson, *On three-dimensional packets of surface waves*, Proc. R. Soc. Lond. A **388**, 101–110 (1974).
- [6] B. Deconinck, M. van Hoeij, *Computing Riemann matrices of algebraic curves*, Physica D, **28**, 152–153 (2001).
- [7] B. Deconinck, M. Heil, A. Bobenko, M. van Hoeij, M. Schmies, *Computing Riemann Theta Functions*, Mathematics of Computation **73**, 1417 (2004).
- [8] B. Deconinck, M. Patterson, *Computing with plane algebraic curves and Riemann surfaces: the algorithms of the Maple package “algcurves”*, in A.I. Bobenko, C. Klein, (ed.), *Computational Approach to Riemann Surfaces*, Lect. Notes Math. **2013** (2011).
- [9] B.A. Dubrovin, *Theta functions and non-linear equations*, Usp. Mat. Nauk **36**, No. 2, 11–80 (1981) (English translation: Russ. Math. Surv. **36**, No. 2, 11–92 (1981)).
- [10] B.A. Dubrovin, *Matrix finite-zone operators*, Revs. Sci. Tech. **23**, 20–50 (1983).
- [11] B. Dubrovin, S. Natanzon, *Real theta-function solutions of the Kadomtsev- Petviashvili equation*, Math. USSR Investiya, **32:2**, 269–288 (1989).
- [12] J. Elgin, V. Enolski, A. Its, *Effective integration of the nonlinear vector Schrödinger equation*, Physica D **225** (22), 127–152 (2007).
- [13] J. Fay, *Theta functions on Riemann surfaces*, Lecture Notes in Mathematics **352** (1973).
- [14] J. Frauendiener, C. Klein, *Hyperelliptic theta functions and spectral methods*, J. Comp. Appl. Math. (2004).
- [15] J. Frauendiener, C. Klein, *Hyperelliptic theta functions and spectral methods: KdV and KP solutions*, Lett. Math. Phys., Vol. **76**, 249–267 (2006).
- [16] J. Frauendiener, C. Klein, *Algebraic curves and Riemann surfaces in Matlab*, in A. Bobenko and C. Klein (ed.), *Riemann Surfaces –Computational Approaches*, Lecture Notes in Mathematics Vol. **2013** (Springer) (2011).
- [17] A. Harnack, *Ueber die Vieltheiligkeit der ebenen algebraischen Curven*, Math. Ann., **10**, 189–199 (1876).
- [18] A.R. Its, *Inversion of hyperelliptic integrals and integration of nonlinear differential equations*, Vestn. Leningr. Gos. Univ. **7**, No. 2, 37–46 (1976).
- [19] C. Kalla, *New degeneration of Fay’s identity and its application to integrable systems*, preprint arXiv:1104.2568v1 (2011).
- [20] C. Kalla, *Breathers and solitons of generalized nonlinear Schrödinger equations as degenerations of algebro-geometric solutions*, preprint arXiv:1106.0154v1 (2011).

- [21] I. Krichever, *The averaging method for two-dimensional integrable equations*, (Russian) Funktsional. Anal. i Prilozhen. **22**, No. 3, 37–52, 96 (1988); translation in Funct. Anal. Appl. **22** (1988), No. 3, 200–213 (1989).
- [22] T. Malanyuk, *Finite-gap solutions of the Davey-Stewartson equations*, J. Nonlinear Sci, **4**, No. 1, 1–21 (1994).
- [23] S. Manakov, *On the theory of two-dimensional stationary self-focusing of electromagnetic waves*, Sov. Phys. JETP **38**, 248 (1974).
- [24] D. Mumford, *Tata Lectures on Theta. I and II.*, Progress in Mathematics, 28 and 43, respectively. Birkhäuser Boston, Inc., Boston, MA, 1983 and 1984.
- [25] R. Radhakrishnan, R. Sahadevan and M. Lakshmanan, *Integrability and singularity structure of coupled nonlinear Schrödinger equations*, Chaos, Solitons and Fractals **5**, No. 12, 2315–2327 (1995).
- [26] T. Shiota, *Characterization of Jacobian varieties in terms of soliton equations*, Invent. Math. , **83** p. 333–382 (1986).
- [27] L.N. Trefethen, *Spectral Methods in Matlab*, SIAM, Philadelphia, PA (2000).
- [28] C.L. Tretkoff, M.D. Tretkoff, *Combinatorial group theory, Riemann surfaces and differential equations*, Contemporary Mathematics, **33**, 467–517 (1984).
- [29] M. Trott, *Applying Groebner Basis to Three Problems in Geometry*, Mathematica in Education and Research **6** (1): 15–28 (1997).
- [30] V. Vinnikov, *Self-adjoint determinantal representations of real plane curves*, Math. Ann. **296**, 453–479 (1993).
- [31] V.E. Zakharov, A.B. Shabat, *Exact theory of two-dimensional self-focusing and one-dimensional self-modulation of waves in nonlinear media*, Sov. Phys. JETP **34**, 62–69 (1972).
- [32] V. Zakharov and E. Schulman, *To the integrability of the system of two coupled nonlinear Schrödinger equations*, Physica D **4**, 270–274 (1982).

INSTITUT DE MATHÉMATIQUES DE BOURGOGNE, UNIVERSITÉ DE BOURGOGNE, 9 AVENUE ALAIN SAVARY, 21078 DIJON CEDEX, FRANCE

E-mail address: `Caroline.Kalla@u-bourgogne.fr`

INSTITUT DE MATHÉMATIQUES DE BOURGOGNE, UNIVERSITÉ DE BOURGOGNE, 9 AVENUE ALAIN SAVARY, 21078 DIJON CEDEX, FRANCE

E-mail address: `Christian.Klein@u-bourgogne.fr`